

See discussions, stats, and author profiles for this publication at: <https://www.researchgate.net/publication/332503492>

# Emerging applications of biochar-based materials for energy storage and conversion

Article in *Energy & Environmental Science* · April 2019

DOI: 10.1039/C9EE00206E

---

CITATIONS

34

---

READS

862

3 authors, including:



[Wu-Jun Liu](#)

University of Science and Technology of China

52 PUBLICATIONS 2,533 CITATIONS

[SEE PROFILE](#)



[Han-Qing Yu](#)

University of Science and Technology of China

719 PUBLICATIONS 26,792 CITATIONS

[SEE PROFILE](#)

Some of the authors of this publication are also working on these related projects:



waster water treatment [View project](#)



bioelectrochemistry [View project](#)



Cite this: *Energy Environ. Sci.*,  
2019, 12, 1751

## Emerging applications of biochar-based materials for energy storage and conversion

Wu-Jun Liu,  Hong Jiang  and Han-Qing Yu \*

Global warming, environmental pollution, and an energy shortage in the current fossil fuel society may cause a severe ecological crisis. Storage and conversion of renewable, dispersive and non-perennial energy from the sun, wind, geothermal sources, water, or biomass could be a promising option to relieve this crisis. Carbon materials could be the most versatile platform materials applied in the field of modern energy storage and conversion. Conventional carbon materials produced from coal and petrochemical products are usually energy intensive or involve harsh synthetic conditions. It is highly desired to develop effective methods to produce carbon materials from renewable resources that have high performance and limited environmental impacts. In this regard, biochar, a bio-carbon with abundant surface functional groups and easily tuned porosity produced from biomass, may be a promising candidate as a sustainable carbon material. Recent studies have demonstrated that biochar-based materials show great application potential in energy storage and conversion because of their easily tuned surface chemistry and porosity. In this review, recent advances in the applications of biochar-based materials in various energy storage and conversion fields, including hydrogen storage and production, oxygen electrocatalysts, emerging fuel cell technology, supercapacitors, and lithium/sodium ion batteries, are summarized, highlighting the mechanisms and open questions in current energy applications. Finally, contemporary challenges and perspectives on how biochar-based materials will develop and, in particular, the fields in which the use of biochar-based materials could be expanded are discussed throughout the review. This review demonstrates significant potential for energy applications of biochar-based materials, and it is expected to inspire new discoveries to promote practical applications of biochar-based materials in more energy storage and conversion fields.

Received 20th January 2019,  
Accepted 18th April 2019

DOI: 10.1039/c9ee00206e

rsc.li/ees

### Broader context

Global warming, environmental pollution, and an energy shortage in the current fossil fuel society may cause a severe global crisis. Storage and conversion of renewable, dispersive and non-perennial energy from the sun, wind, geothermal sources, water, or biomass could be a promising option to relieve this crisis. Biochar, a carbon-rich solid residue formed in the pyrolysis of biomass, could be one of the most versatile platform materials applied in the field of modern energy storage and conversion because of its easily-tuned surface chemistry and porosity as well as abundant availability and carbon-neutral nature. Recently, the application potential of biochar-based materials in hydrogen storage and conversion, oxygen electrocatalysis, emerging fuel cell technologies, supercapacitors and lithium/sodium ion batteries has been extensively explored, but the low biomass conversion efficiency, impurity of biochar and poor flexibility severely limit their practical feasibility. Here, we provide critical rethinking about the challenges and opportunities of biochar-based materials in the energy storage and conversion fields, and propose a more promising avenue for their applications. The merits and demerits of biochar-based materials as a functional energy material are analyzed, and the design and synthesis of high-performance biochar-based materials as well as their scaled-up applications in the emerging energy storage and conversion fields are presented.

## 1. Introduction

The contradiction of ever-increasing global energy demand and declining of fossil fuel sources such as petroleum, coal, and natural gas has posed serious challenges to energy security,

climate change, and even society and political stability. It is imperative to develop cost-effective and environmentally friendly solutions to meet and address these challenges. In this regard, storage and conversion of the renewable, dispersive and non-perennial energy from the sun, wind, earth, water, or biomass should be an effective option.<sup>17</sup> The development of high-performance and cost-effective materials is crucial for the efficient implementation of the energy storage and conversion process.<sup>25</sup> Ideally, these materials should be industrially and

CAS Key Laboratory of Urban Pollutant Conversion, Department of Applied Chemistry, University of Science & Technology of China, Hefei, 230026, China.  
E-mail: hqyu@ustc.edu.cn

economically attractive (*e.g.*, readily scalable and cost-effective) and synthesized from renewable and naturally abundant resources. Carbon is the most widespread and second-most abundant element (after oxygen) in the biosphere of the earth, and it provides a basis for the storage of renewable energy in the form of carbohydrates and other biopolymers. Meanwhile, carbon-based materials have played important roles in recently emerging energy conversion and storage processes,<sup>31</sup> including hydrogen storage and production,<sup>32–34</sup> oxygen electrocatalysts for fuel cells,<sup>35,36</sup> and electrodes in energy storage devices such as supercapacitors and lithium ion batteries.<sup>39,40</sup> As a consequence, carbon materials and their energy applications have become a very important topic recently in the field of sustainable chemistry, and studies are quickly developing.<sup>49</sup>

Conventionally, most functional carbon-based materials (*e.g.*, activated carbon, carbon nanofibers/tubes, and graphene) are produced from coal or petrochemical products through energy-intensive or harsh synthetic processes.<sup>50–53</sup> For example,



**Wu-Jun Liu**

*Wu-Jun Liu received his PhD degree from the University of Science & Technology of China (USTC) under the supervision of Prof. Han-Qing Yu in 2014. He is now an associate research fellow at USTC. His research field is green chemistry and energy, focusing on the sustainable conversion of biomass waste into value-added chemicals and biochar. To date, he has published more than 30 papers on this research topic in peer-reviewed international journals.*



**Hong Jiang**

*Hong Jiang obtained his PhD degree in Applied Chemistry from USTC in 2004. From 1999, he joined USTC, and is presently an Associate Professor of applied chemistry. His recent research interests include biomass refinery, preparation of biomass-based carbonaceous materials, and functionalization of biomass materials.*



**Han-Qing Yu**

*Han-Qing Yu is currently a professor in the Department of Applied Chemistry, USTC. He received his PhD from Tongji University, China in 1994. After that, he worked as a Marie Curie postdoctoral fellow at the University of Newcastle upon Tyne in the UK, a research fellow at the Nanyang Technological University, and a research assistant professor at the Hong Kong University. He is now an editorial board member*

*of eight international journals. His research interests include contaminant degradation and nanomaterials for environmental application. He has published more than 400 international peer-reviewed papers and 8 invited book chapters.*

activated carbon is usually produced from coal or other non-renewable resources *via* different activation processes such as steam/CO<sub>2</sub> activation or chemical (*e.g.*, ZnCl<sub>2</sub>, H<sub>3</sub>PO<sub>4</sub>, and KOH) activation. Carbon nanomaterials like carbon nanofibers/tubes and graphene are usually produced from the chemical vapor deposition or electric-arc discharge techniques. Chemical vapor deposition (CVD) is a deposition method using gaseous petrochemical products (*e.g.*, ethylene, methane, acetylene, and hydrogen gas) as a carbon resource to produce high-quality carbon-based materials such as graphene or carbon nanotubes/fibers at high temperatures (usually higher than 800 °C). Unlike the CVD method, the electric-arc discharge technique can use solid carbon raw materials such as coal or graphite as a carbon resource to produce high-quality carbon nanotube materials. Both the CVD and electric-arc discharge techniques usually involved high temperature and complicated operational processes.<sup>63,64</sup> These disadvantages greatly suppress their large scale production and industrial applications. Thus, the development of effective methods to produce carbon materials from renewable resources with high performance and limited environmental impacts is greatly needed. From the view of sustainable carbon material (biochar) production, biomass should be a promising raw material for the synthesis of various biochar-based materials due to its renewable nature and natural abundance.

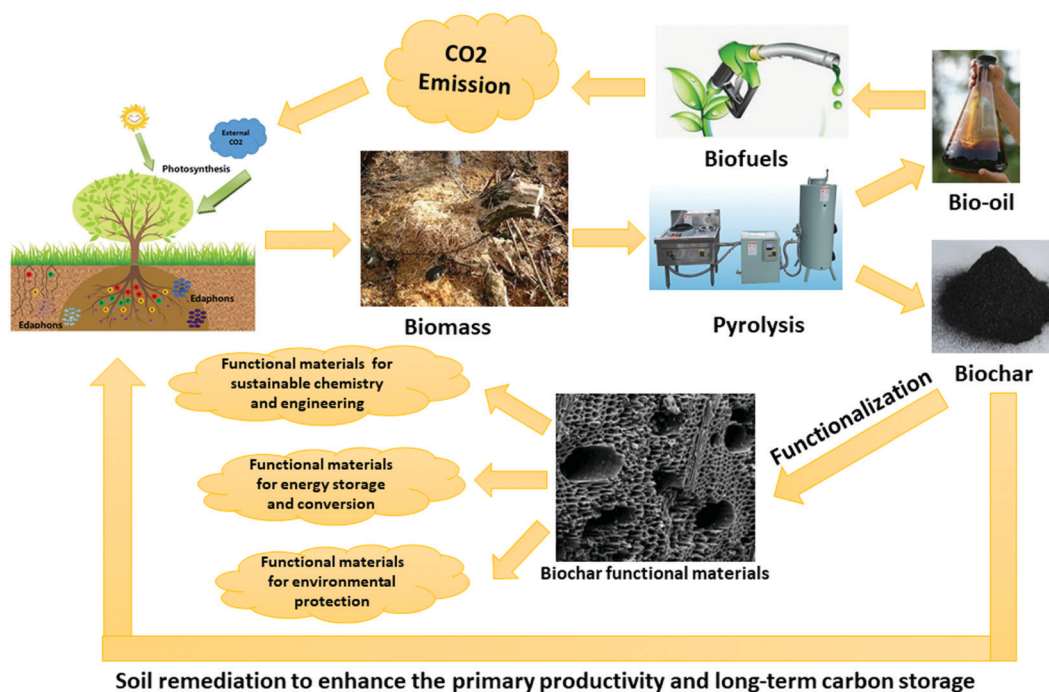
The global annual biomass production is more than  $2 \times 10^{11}$  tons (dry carbon basis) as estimated in 2016.<sup>70</sup> Accordingly, developing flexible approaches to prepare sustainable carbon materials from biomass is becoming a research focus. Biochar, also called bio-carbon, is a solid residue produced from the thermal decomposition of biomass at moderate temperatures (usually 350–700 °C) without oxygen or with a limited oxygen supply. Such a definition distinguishes biochar from conventional carbon materials like activated carbon and carbon black, which are mainly produced from coal or petroleum based resources. Table 1 presents the main differences among

**Table 1** Comparison of biochar with activated carbon and carbon black (reprinted with permission from ref. 77, Copyright 2015, American Chemical Society)

	Biochar	Activated carbon	Carbon black
Precursors	Biomass	Coal, asphalt, and biomass <i>etc.</i>	Petroleum, coal tar, and asphalt, <i>etc.</i>
Carbon content	40–90%	80–95%	> 95%
Structure features	Amorphous carbon with abundant surface functional groups, nanostructures, or porosity	Amorphous carbon with abundant porosity	Microcrystal or amorphous carbon particles
Preparation method	Pyrolysis of the biomass at medium temperature (400–600 °C), then functionalization with physical or chemical methods	Carbonization of the coal, asphalt or biomass at high temperature (700–1000 °C) under physical or chemical activation	Combustion of petroleum, coal tar, or asphalt under air-poor conditions

biochar, activated carbon, and carbon black. Both biochar and activated carbon have an amorphous carbon matrix with abundant porosity, but there is no fundamental difference between them. Activated carbon materials produced from biomass could even be regarded as biochar essentially. However, the main difference between biochar and activated carbon is that the surface of biochar is usually rich in functional groups.<sup>77</sup> Compared with fossil-fuel-based activated carbon and carbon black, the large scale production of biochar should be regarded as a sustainable process, as anthropogenic CO<sub>2</sub> emissions can be mitigated in the production of biochar from biomass. The sustainable concept for biochar production is displayed in Fig. 1.<sup>82</sup> The CO<sub>2</sub> in the atmosphere can be fixed into biomass through the photosynthesis of green plants. In the biochar production process, the fixed CO<sub>2</sub> is bound to the carbon matrix of biochar, providing an efficient way to remove CO<sub>2</sub> from the carbon cycle and thus remitting global warming. In this way, 0.1–0.3 billion tons of CO<sub>2</sub> can be removed from the carbon cycle by carbon storage in biochar.<sup>1</sup>

Biomass is composed of cellulose, hemicelluloses, and lignin. Hemicellulose (15–30 wt% of biomass) is an amorphous branched polymer consisting of mainly pentoses, hexoses, and uronic acids. It decomposes first, at about 200–260 °C, in biomass pyrolysis.<sup>89</sup> Cellulose (40–50 wt% of biomass) is a homopolymer with only β-glycosidic bond linked β-D-glucopyranose units, and it decomposes following the hemicellulose, at about 240–350 °C.<sup>90,91</sup> Lignin (15–30 wt% of biomass) consists of three primary monomers, *i.e.*, coniferyl alcohol, sinapyl alcohol, and *p*-coumaryl alcohol, and it breaks up at 280–500 °C.<sup>92</sup> Since hemicellulose, cellulose, and lignin could decompose at temperatures lower than 500 °C, biomass could be easily pyrolyzed at low temperatures, producing bio-oil, incondensable gas, and biochar. However, the biochar-based materials obtained from the low-temperature pyrolysis of biomass don't work well in some energy storage and conversion fields, including Li/Na ion batteries and so on, due to their low surface areas and poor pore features. Thus, before their applications, a pre-functionalization process, such as surface modifications and activation, should be conducted. For more

**Fig. 1** Schematic illustration of sustainable concepts in the production of biochar and its impact on global climate.

information about the details of the biochar production and functionalization processes, the reader can refer to some excellent reviews published previously.<sup>95,96</sup> Biochar-based functional materials offer many advantages in energy storage and conversion applications due to its easily tuned porosity and surface chemistry. From the view of the mechanism, energy storage and conversion involve mainly physical interaction and chemical reactions at the interface and/or surface.<sup>25</sup> As a result, the porosity and surface functional groups could play an important role in energy storage and conversion processes. For example, the surface functional groups (surface chemistry and surface energy) have great effects on the thermodynamics of the heterogeneous reactions happening at the interface when phase transitions are involved in the energy storage and conversion processes, while the surface porosity can limit the kinetics and rate of physical interaction and chemical reactions.<sup>98</sup> Meanwhile, the easily tuned porosity and surface chemistry of biochar also make it a versatile platform for the preparation of many biochar-nanostructured composites, which could also be employed as materials for energy storage and conversion applications. For more detailed information on how to tune the porosity and surface chemistry as well as prepare biochar-nanostructured composites, which is out of the scope of this review, the readers can refer to one of our previous reviews and the references therein.<sup>77</sup>

During the past few decades, there has been an increasing awareness of the potential of biochar to provide an efficient and versatile platform for various applications, mainly in the environmental and catalysis fields. For example, the applications of biochar in soil remediation and the improvement of environmental quality have been reviewed comprehensively by Manyà *et al.*,<sup>99</sup> Meyer *et al.*,<sup>100</sup> Laird *et al.*,<sup>95</sup> and Hyland and Sarmah,<sup>101</sup> while the catalytic application of biochar has been summarized more recently by Lee *et al.*,<sup>102</sup> and Xiong *et al.*<sup>103</sup> In addition, several reviews exist on the application of biomass-derived carbon materials in some specific energy applications. For example, Abioye and Ani<sup>104</sup> reviewed recent developments of carbon materials produced from waste biomass for supercapacitors, while Long *et al.*,<sup>105</sup> and Yao *et al.*,<sup>106</sup> summarized the application of nanostructured carbons derived from biomass as anode materials for lithium/sodium ion batteries. Apart from supercapacitors and lithium/sodium ion batteries, biochar-based materials have also been used in other energy applications, such as hydrogen storage and production, oxygen electrocatalysts, and fuel cells. However, no systematic and critical review covering the applications of biochar-based materials in all of these aspects of energy storage and conversion has been available until now. As biochar-based materials have been widely applied in various energy storage and conversion processes, it is not only very necessary but also timely to comprehensively review the applications of biochar-based materials in all aspects of energy storage and conversion technologies; this could provide some direction on the future development of the applications of biochar-based materials. Therefore, this review aims to provide a critical overview on the research advancements, highlighting the most recent developments and the limitations of biochar-based

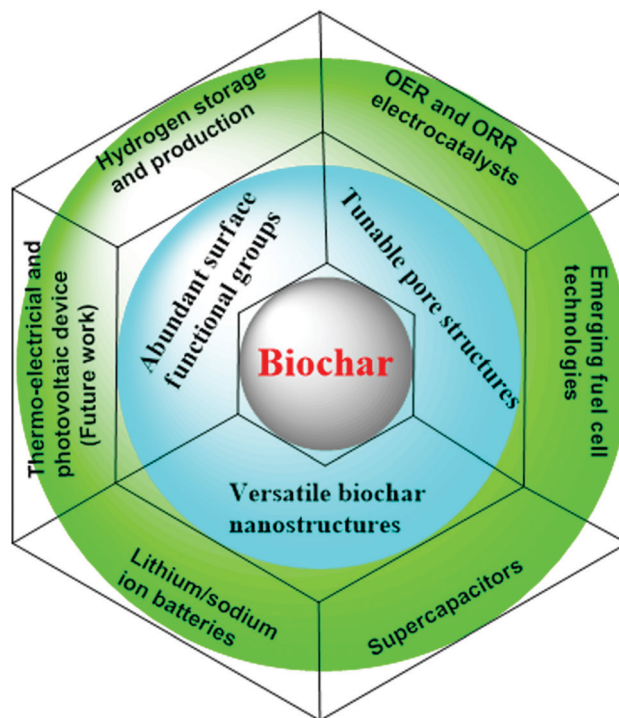


Fig. 2 Summary of features of biochar based functional materials and their application in various energy storage and conversion fields.

materials in energy storage and conversion applications. We would like to provide the reader with comprehensive information and different perspectives on biochar-based materials for energy storage and conversion applications (Fig. 2).

Specifically, this review will discuss the following topics: (1) biochar-based materials for hydrogen storage and production; (2) the applications of biochar-based materials as oxygen reduction and evolution electrocatalysts; (3) biochar-based materials for emerging fuel cells; (4) biochar-based materials for supercapacitor electrodes; and (5) biochar-based materials for lithium/sodium ion batteries. These five topics were selected for this review because they cover nearly all of the aspects of energy storage and conversion in which biochar-based materials can be applied. Furthermore, although these five topics address different fundamental and technical challenges, they are connected through the common use of biochar-based materials to form mass/electron transport or electrodes involving solid-liquid interfaces.

## 2. Biochar-based materials for hydrogen energy

Hydrogen ( $H_2$ ) is a promising energy carrier because of its high energy density and wide availability and abundance. The gravimetric energy output for  $H_2$  combustion ( $120 \text{ MJ kg}^{-1}$ ) is almost 3 times higher than that of gasoline ( $44.5 \text{ MJ kg}^{-1}$ ), leaving only water as the final product after energy output.<sup>107</sup> Benefiting from these features,  $H_2$  energy can act as an on-board fuel, attracting much attention in terms of  $H_2$  storage and the  $H_2$

evolution reaction (HER); therefore, the H<sub>2</sub> energy economy has recently been regarded as one of the most ideal approaches to address the upcoming fossil fuel exhaustion and the ever-worsening environmental pollution and global warming.<sup>108</sup>

## 2.1 Hydrogen storage

Recently, hydrogen infrastructure in terms of production and storage has served a critical role in the commercialization of fuel cells. One of the main obstacles hindering the commercial application of H<sub>2</sub> in fuel cell systems is the storage of sufficient H<sub>2</sub> in a sustainable and cost-effective way.<sup>17,109</sup> Among all of the conventional methods for H<sub>2</sub> storage,<sup>110</sup> namely, chemical storage, physical adsorption, liquefaction and gas compression, physical adsorption offers several advantages such as relatively high storage capacity, reversibility, and rapid kinetics.<sup>111</sup> Carbon-based porous materials have been extensively investigated as potential H<sub>2</sub> physical adsorption materials due to their high surface area, large pore volume, good chemical stability, and easily tailored porosity.<sup>112</sup> In general, the use of porous carbon-based materials can decrease the gravimetric and volumetric storage densities; more importantly, the increased surface area and porosity of the carbon can offer additional binding sites on the surface and in the pores, thus enhancing their H<sub>2</sub> storage performance. However, porous carbon materials synthesized from coal or petroleum sources *via* conventional heat treatment usually have a large amount of mesopores and macropores (more than 50% of the total pore volume) with a pore dimension greater than 4 nm.<sup>113</sup> The mesopores and macropores can only come into play in a monolayer adsorption manner, which is similar to hydrogen bound on a plane, and thus are not very efficient for ambient-temperature H<sub>2</sub> storage.<sup>114,115</sup>

Biochar, an engineered carbon material with tunable pore structure and surface functional groups, has been used for hydrogen-storage applications. Biochar has a high surface area with abundant micropore features *via* KOH, ZnCl<sub>2</sub> or steam activation (for detailed information on how to tune the pore structure of biochar, the readers could refer to one of our previous review papers<sup>77</sup> and references therein). The micropore structure is regarded as a main contribution to H<sub>2</sub> adsorption due to its capillarity forces, which could significantly reduce the H<sub>2</sub> adsorption-potential.<sup>116</sup> Thus, biochar materials could be a promising alternative to conventional activated carbon for high efficient H<sub>2</sub> adsorption. Meanwhile, compared to conventional coal or petroleum derived activated carbon materials, the abundant surface functional groups or inorganic species (*e.g.*, alkali or alkali-earth metals) of biochar could also be big supplement to its high performance in H<sub>2</sub> storage due to the contribution of chemisorption.<sup>117</sup> For example, K<sup>+</sup> or Na<sup>+</sup> species, which are commonly found in biochar materials, could act as alkaline cores to attract H<sub>2</sub>, and the abundant sp<sup>2</sup> carbon framework in biochar could separate charge from the alkali metal ions due to its high electron affinity, providing strong stabilization to the adsorbed molecular H<sub>2</sub>.

Because of the above advantages, various biochar materials with high micropore content, and abundant surface functional

groups have been extensively explored as H<sub>2</sub> storage media. For example, a biochar material with tunable morphology and texture was synthesized by KOH activation of melaleuca bark biomass,<sup>118</sup> which has a high surface area (up to 3170 m<sup>2</sup> g<sup>-1</sup>), a large micropore volume (0.86 cm<sup>3</sup> g<sup>-1</sup>), and abundant surface oxygenous groups, and thus demonstrates a large H<sub>2</sub> storage capacity (4.08 wt% at 77 K and 1 MPa). Zhang and co-workers<sup>119</sup> prepared microporous carbon (MC) with a high surface area and large micropore volume from cornstalks *via* pyrolysis and KOH activation. The MC exhibited favorable H<sub>2</sub> storage performance with a maximum H<sub>2</sub> adsorption capacity of 4.4 wt% at 77 K, and it also showed good selectivity towards CH<sub>4</sub> and CO<sub>2</sub>. Such a high adsorption capacity and good selectivity for H<sub>2</sub> could be attributed to its abundant micropore structure and high surface area. By adjusting the reaction parameters, a series of carbon materials with controlled morphologies and textures were prepared through pyrolysis and activation of biomass waste,<sup>120</sup> and the as-synthesized MCs exhibited high surface areas (2000–3100 m<sup>2</sup> g<sup>-1</sup>), large micropore volumes (1.11–1.68 cm<sup>3</sup> g<sup>-1</sup>), and narrow pore-size distributions (0.77–0.91 nm). A considerable H<sub>2</sub> storage capacity of more than 5 wt% and an isosteric adsorption heat of 4.1–7.5 kJ mol<sup>-1</sup> were obtained by MC at cryogenic temperatures over the pressure range of 0–1 MPa.

Compared with H<sub>2</sub> stored at cryogenic temperatures, room temperature H<sub>2</sub> is more attractive. The tendency for the physisorption of H<sub>2</sub> stored in porous carbons means that the H<sub>2</sub> storage capacity at ambient temperature is often very low, and enhanced H<sub>2</sub> storage can only be realized at a very high pressure.<sup>121</sup> Many efforts to store H<sub>2</sub> at near-ambient temperature have been attempted using biomass-derived porous carbons. For example, the H<sub>2</sub> storage performance of a series of porous carbons derived from coconut shell biomass under room temperature (25 °C) and high pressure (10 MPa) was investigated, and the relationship between the H<sub>2</sub> storage capacity and the textural features of the porous carbon was established.<sup>122</sup> The H<sub>2</sub> storage capacities exhibited relatively linear relationships with properties such as specific surface area and micropore volume. A maximum H<sub>2</sub> storage capacity of 0.85 wt% was obtained for these materials at 10 MPa and 25 °C.

Though biochar has fast adsorption and desorption kinetics and almost complete reversibility, its maximum H<sub>2</sub> adsorption capacity is less than 1 wt% at room temperature even under 100 bar of H<sub>2</sub> pressure. The intrinsic low adsorption enthalpy for H<sub>2</sub> on porous carbon should be a main cause for such a low hydrogen adsorption capacity.<sup>112</sup> Remarkable enhancement in H<sub>2</sub> storage at room temperature can be achieved by using metal-decorated porous carbon materials.<sup>123,124</sup> Hydrogen spillover effects should contribute mainly to the enhanced H<sub>2</sub> adsorption performance of metal-decorated porous carbon materials, which can be broadly defined as the diffusion of dissociated H<sub>2</sub> adsorbed on a first surface onto another surface.<sup>125</sup> The first surface is usually the decorated metal species, which could dissociate the adsorbed H<sub>2</sub>, while the second surface is the porous carbon on which the metal species become decorated. Hydrogen spillover is an important phenomenon for various metal catalyzed hydrogenation reactions,

but now it is accepted that H<sub>2</sub> spillover could also play a critical role in room temperature H<sub>2</sub> storage.<sup>126</sup> Spillover effects could facilitate the surface diffusion of H<sub>2</sub> from the metal sites into the porous carbon matrix in the form of dissociated atomic hydrogen, thus remarkably reducing the adsorption potential at room temperature, and improving the H<sub>2</sub> storage capacity of metal metal-decorated porous carbon materials.

With the spillover effect, significant enhancement in the H<sub>2</sub> storage capacity at room temperature has been obtained for various metal-decorated porous carbon materials. For example, Pd-decorated sepiolite-derived carbon materials were found to exhibit H<sub>2</sub> storage capacities 4 times higher than that of the raw carbon material without Pd doping at room temperature.<sup>127</sup> In addition to the significant improvement in H<sub>2</sub> storage capacity, the Pd NP-doping of wood-derived ultramicroporous carbon can also greatly increase the H<sub>2</sub> uptake rate by decreasing the activation energy of the adsorption process.<sup>128</sup> The embedding of Pd and Pt NPs into biochar can definitely enhance its performance in room temperature H<sub>2</sub> storage, but many problems may arise from the increased sensitivity toward air and moisture as well as the reduced surface area and pore volume caused by blocking the pores with the embedded NPs.<sup>129</sup> Other more recent studies on the applications of biochar-based materials for H<sub>2</sub> storage are summarized in Table 2.

Though biochar based materials have been extensively applied for hydrogen storage, there are still many different challenges, such as reversibility, high dehydrogenation temperature, and strict thermal management. Appropriately designed and synthesized biochar-based materials could have desired thermal conductivity to mediate the absorbed or released heat of dehydrogenation or hydrogenation during the hydrogen storage process. However, one must keep in mind that the discovery of an embedded-metal biochar with a large surface area and high H<sub>2</sub> adsorption energy at room temperature does not guarantee that it will be applied as an effective H<sub>2</sub> storage material. If an adsorbent is to be used in

industry, it should be stable under general working conditions and comparatively insensitive toward moisture, air, and other gas impurities. We can expect that highly stable biochar-based H<sub>2</sub> adsorbents with a large surface area and pore volume, together with many open metal sites and embedded metal NPs for H<sub>2</sub> spillover, should provide some positive results for H<sub>2</sub> storage at ambient temperature.

## 2.2 Hydrogen production

Biochar-based materials not only play an important role in hydrogen storage but also can have applications in hydrogen production, mainly in the production of biological H<sub>2</sub>, electrocatalysis, and the evolution of photocatalytic H<sub>2</sub>.

**2.2.1 Biological H<sub>2</sub> production.** Biological processes, such as fermentation (anaerobic digestion) and microbial photosynthesis, can produce H<sub>2</sub> from low-cost and naturally abundant organic waste and biomass. During anaerobic digestion, microorganisms can form biofilms to break down organic matter, and the biofilms become attached to the surface of either the suspended solid materials or the insoluble organic matter,<sup>130,131</sup> facilitating the growth of microorganisms, thus increasing the H<sub>2</sub> production efficiency. In anaerobic H<sub>2</sub> production, biochar can serve as an additive to increase H<sub>2</sub> production because of its ability to mitigate acid and ammonia inhibition and promote bio-film formation.<sup>132,133</sup> In particular, biochar could support the bacterial growth in the anaerobic digestion process and maintain the stability of cultures due to its high pH buffer capacity, allowing a shorter H<sub>2</sub> production duration and lag phase. As a result, a higher H<sub>2</sub> production rate and yield were obtained compared to the cultures without biochar.<sup>134,135</sup> Meanwhile, interspecies electron transfer (IET) plays critical roles in anaerobic digestion for H<sub>2</sub> production, which can be greatly improved by biochar due to its abundant surface redox active moieties such as quinones and phenazines.<sup>136,137</sup>

Table 2 Summary of the applications of biochar-based materials in H<sub>2</sub> storage and production

Original biomass	Biochar synthesis methods	Applications	Performance	Ref.
Coffee beans	Pyrolysis of the coffee beans at 500 °C for 1 h, then activated with steam at 800 °C for 2 h or with KOH at 850 °C for 2 h	H <sub>2</sub> storage	H <sub>2</sub> storage capacity: 4.0 wt% at 77 K; 0.6 wt% at 298 K	4
Wood biomass	Pyrolysis of the wood biomass with H <sub>3</sub> PO <sub>4</sub> , then activated with KOH	H <sub>2</sub> storage	H <sub>2</sub> storage capacity: 0.8 wt% at 298 K under 2 MPa	11
Corn cob biomass	Pyrolysis of the corn cob biomass at 450 °C for 4 h, then activated with KOH, K <sub>2</sub> CO <sub>3</sub> , or NaOH at 850 °C for 2 h	H <sub>2</sub> storage	H <sub>2</sub> storage capacity: 2.0 wt% at 77 K; 0.6 wt% at 298 K	16
Hemp stems	Pyrolysis of the hemp stems biomass with KOH at 500–800 °C for 2–4.5 h	H <sub>2</sub> storage	H <sub>2</sub> storage capacity: 3.28 wt% at 77 K	22
Peanut shell	Pyrolysis of the peanut shell biomass at 800 °C for 5 h, then activated with KOH at 800 °C	H <sub>2</sub> storage	H <sub>2</sub> storage capacity: 1.2 wt% at 298 K under 0.1 MPa	28
Cellulose	Hydrothermal carbonization of the cellulose at 250 °C for 2 h, then activated with KOH at 600–800 °C for 2 h	H <sub>2</sub> storage	H <sub>2</sub> storage capacity: 8.9 wt% at 77 K under 3 MPa	37
Starch	Heat treatment of Fe <sub>3</sub> O <sub>4</sub> /starch mixture at 400 °C for 4 h without oxygen	Biological H <sub>2</sub> production	Maximum H <sub>2</sub> yield of 218.63 mL H <sub>2</sub> per g glucose	44
Pine needles	Pyrolysis of the pine needle biomass at 600 °C for 1 h, then activated with KOH at 700–900 °C	Electrocatalytic H <sub>2</sub> evolution	Onset potential: 4 mV; Tafel slope: 45.9 mV dec <sup>-1</sup>	54
Chitosan	Pyrolysis of the mixture of NaCl, chitosan and ammonium molybdate 850 °C for 3 h under Ar/H <sub>2</sub> to obtain Mo <sub>2</sub> C@N-C nanosheets	Electrocatalytic H <sub>2</sub> evolution	Overpotential of 210 mV for 10 mA cm <sup>-2</sup> ; Tafel slope: 69 mV dec <sup>-1</sup>	60
Willow catkins	Pyrolysis of the willow catkin biomass at 600 °C for 1 h, then loaded with cobalt(II) acetylacetonate and pyrolysis at 700–900 °C to obtain Co <sub>3</sub> O <sub>4</sub> -biochar nanocomposites	Electrocatalytic H <sub>2</sub> evolution	Overpotential of 0.21 V for 10 mA cm <sup>-2</sup>	68

As reported by Sharma *et al.*,<sup>132</sup> a maximum H<sub>2</sub> yield of 96.63 ± 2.8 mL H<sub>2</sub> per g carbon is achieved with the addition of biochar to the anaerobic digestion system compared with 22.55 ± 2.2 mL H<sub>2</sub> per g carbon without biochar. Zhang *et al.*<sup>21</sup> also found that with the addition of biochar and a suitable concentration of Fe<sup>2+</sup> the H<sub>2</sub> production from glucose increased from 158.0 to 234.4 mL g<sup>-1</sup> glucose while the lag phase time decreased from 4.25 to 2.12 h. During anaerobic H<sub>2</sub> production, biochar can act as support carriers of anaerobes and a system pH buffer, promoting biofilm formation and maintaining a suitable system pH environment and thus increasing the growth of the anaerobes; meanwhile, a suitable Fe<sup>2+</sup> concentration can improve the hydrogenase activity of the anaerobes, and these synergistic effects of biochar and Fe<sup>2+</sup> increase the H<sub>2</sub> production and shorten the lag time. Apart from bacteria immobilization and pH buffering, biochar can also provide several other benefits for anaerobic H<sub>2</sub> production. For example, the trace inorganic species and volatile matter contained in biochar could provide temporary nutrients for the growth of fermentative bacteria.<sup>138</sup>

**2.2.2 Electrocatalytic H<sub>2</sub> evolution.** Apart from biological H<sub>2</sub> production, electrocatalytic water splitting is an alternative approach to existing catalytic systems using fossil fuels for the production of high-purity H<sub>2</sub>. During the hydrogen evolution reaction (HER), electrocatalysts are essential to decreasing the overpotential and achieving high catalytic current densities. Efficient catalytic HER from water under the catalysis of biochar-based materials has emerged as another important approach to producing clean and renewable H<sub>2</sub> fuel. The integration of catalytically active species into biochar should be an effective route to developing high-performance HER electrocatalysts.<sup>139–143</sup> For example, Zhou *et al.*<sup>10</sup> demonstrated that sulfur- and nitrogen-doped biochar derived from peanut root nodule biomass can act as an efficient electrocatalyst for the HER. The as-synthesized material (porous N- and S-doped carbon, PNSC) exhibits a porous and multilayered structure, with well-distributed N, S, and C (Fig. 3a–c) and a high electrochemical area of 27.4 mF cm<sup>-2</sup>. PNSC shows excellent HER catalytic performance with an on-set potential of 27 mV, only 4 mV more negative than that of the commercial 20 wt% Pt/C catalyst, a Tafel slope of 67.8 mV dec<sup>-1</sup> and good catalytic stability (Fig. 3d–f). Density functional theory (DFT) calculations indicated that both S and N doping can remarkably alter the electronic structure of the carbon matrix and increase the electron density of the surrounding carbon atoms. The S and N atoms can also enhance the interaction between the catalyst and H<sup>+</sup> due to their lone-pair electrons and subsequently efficiently increase the HER activity of biochar-based materials (Fig. 3g).

Further on this work, an S- and N-doped biochar derived from sunflower seed shell biomass was integrated with Mo<sub>2</sub>C nanoparticles to form a biochar-nanostructured composite, which needs an overpotential of only 60 mV to deliver a current density of 10 mA cm<sup>-2</sup>. Meanwhile, due to its particular structural features, the catalyst also had outstanding durability and a faradaic efficiency of nearly 100%.<sup>144</sup> In another case, a

carbon fiber aerogel derived from cotton wool biomass acted as a support for the growth of MoSe<sub>2</sub> nanosheets (MoSe<sub>2</sub>/CFA), and the as-synthesized material shows excellent electrochemical activity as a HER electrocatalyst with a small onset potential of 104 mV vs. RHE and a Tafel slope of 62 mV dec<sup>-1</sup>.<sup>145</sup> For more recent studies on the applications of biochar for hydrogen production, please see Table 2.

Although biochar-based materials have found their application in electrocatalytic hydrogen evolution, some challenges still need to be addressed. (1) The HER catalytic mechanism of heteroatom-doped biochar or biochar-nanostructured composites should be clarified, and the actual active catalytic sites should be discerned. For this purpose, *in situ* high-resolution spectroscopic, microscopic, and electrochemical techniques combined with advanced theoretical calculations could help to fully illuminate the reaction mechanism and identify the actual active catalytic sites. (2) After the identification of the active catalytic sites and the illumination of the mechanism, increasing the number of active catalytic sites in the materials should be investigated. A more advanced synthesis should be developed to prepare biochar-based materials with good atomic dispersion of the doping heteroatoms or nanostructure, and single-atom-based catalysts are overwhelmingly preferred.

### 3. Biochar-based materials for oxygen electrocatalysts

The oxygen reduction and evolution reactions (ORR and OER) are two of the most important reactions occurring in electrochemical energy storage and conversion processes, such as in fuel cells, water splitting, and metal–air batteries.<sup>146–148</sup> The efficiencies of the ORR and OER are significantly restricted by the sluggish reaction kinetics of oxygen species, and efficient catalysts are required to overcome the energy barrier. Conventional electrocatalysts for the ORR and OER are mainly based on noble metals and their oxides (such as Pt, Pd, RuO<sub>2</sub>, and IrO<sub>2</sub>). However, poor stability under operating conditions as well as high cost and scarcity seriously limit their large-scale commercial applications. Due to their low cost, abundance, and availability, biochar-based materials are widely explored for the ORR and OER in energy storage and conversion devices. A detailed discussion of these aspects is presented in this section.

#### 3.1 Oxygen reduction reaction

The ORR is a key process in fuel cells and metal–air batteries, and it is recognized as a main limiting factor of the energy-conversion efficiency in these devices.<sup>35,149</sup> Traditionally, platinum (Pt) and its alloys are the most effective ORR catalysts.<sup>150</sup> Unfortunately, extremely low abundance and high costs have greatly hindered the wide application of Pt-based catalysts in fuel cells and metal–air batteries. Moreover, apart from facing prohibitively low abundance and high costs, Pt-based ORR catalysts also suffer many other problems, such as poor long-term stability and low methanol and CO tolerances.<sup>151</sup> Therefore, the development of alternative, cost-effective, high abundance catalysts with favorable

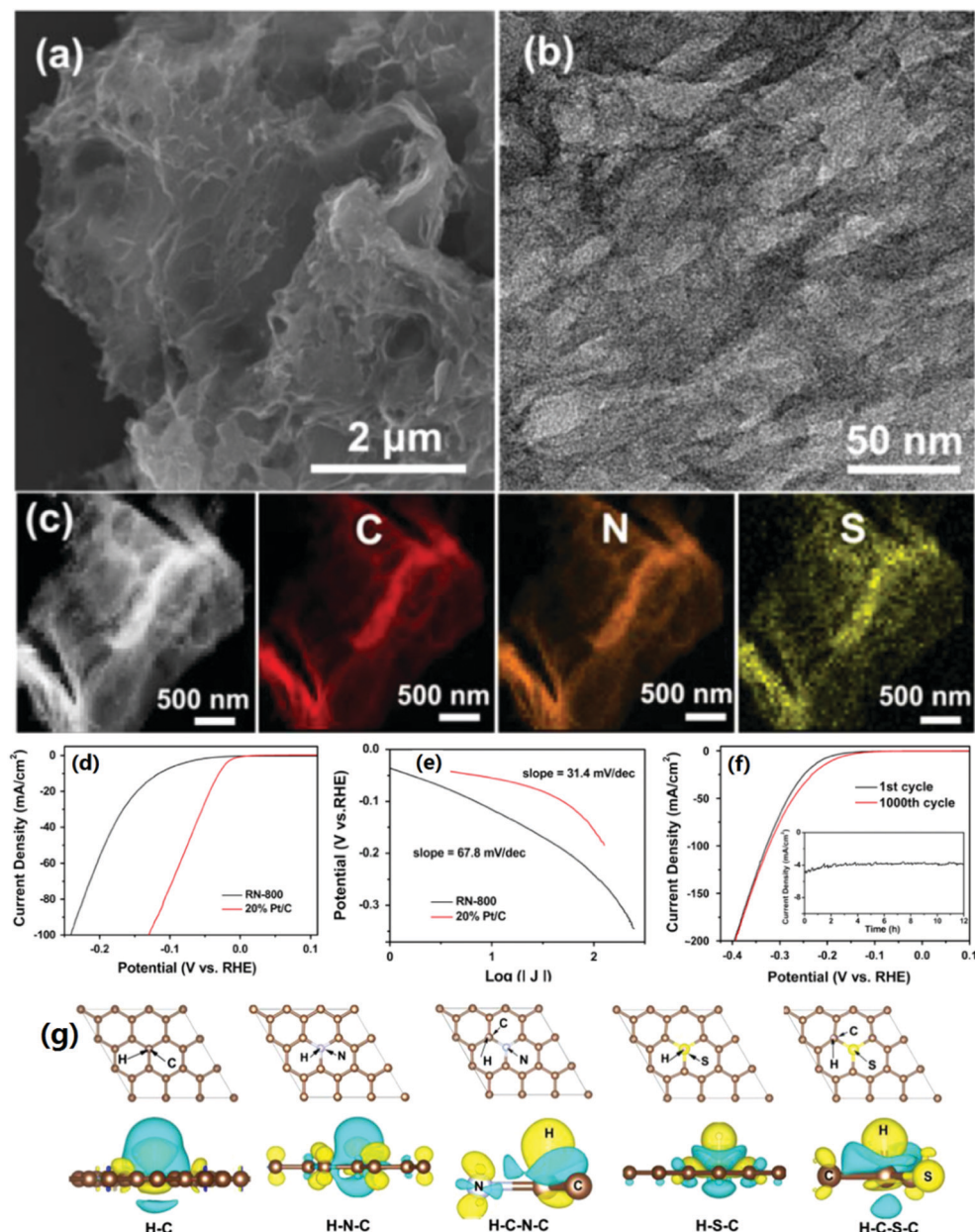
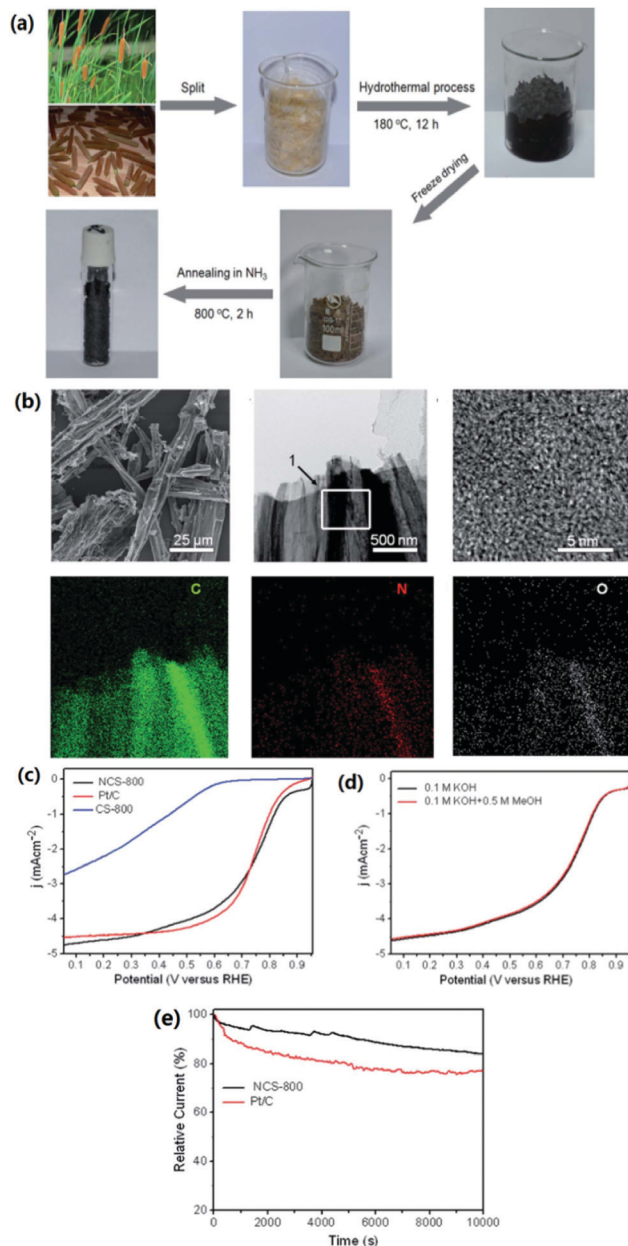


Fig. 3 (a) SEM image, (b) TEM image, and (c) EDS maps of the PNSC; (d) polarization curves, (e) Tafel plots, and (f) cycle performance of the PNSC in the HER; and (g) the DFT calculation for the HER process. (Reprinted with permission from ref. 10, Copyright 2015, Elsevier Co.).

catalytic ORR activity, long-term stability, and high methanol and CO tolerances is essential for the development of fuel cells and metal–air batteries. Biochar-based materials (e.g., heteroatom-doped porous biochar materials and biochar-nanostructured composites) can afford advanced matrices with a high surface area and implanted active catalytic sites, such as doped heteroatoms and active metal sites.<sup>152</sup>

Some lignocellulosic biomass usually contains high levels of heteroatoms such as N, S, and P, and it is a promising precursor for the direct production of heteroatom-doped carbon materials, which then act as highly efficient ORR catalysts. Among them, nitrogen-doped biochar materials are the most widely used ORR electrocatalysts. For example, by hydrothermally treating

*Typha orientalis* biomass at 180 °C to obtain biochar and following pyrolysis of the biochar under NH<sub>3</sub> gas conditions (Fig. 4a), Chen *et al.*<sup>153</sup> successfully prepared a N-doped carbon nanosheet with a nonporous, 3D interpenetrated network structure and well-doped N (Fig. 4b). The as-synthesized carbon materials show excellent catalytic activity toward the ORR in both acidic and alkaline media, with the onset potential and half-wave potential being similar to those of commercial 20 wt% Pt/C (Fig. 4c) and a calculated electron transfer number during the ORR process of approximately 4 from 0.055 to 0.900 V (*vs.* RHE). Furthermore, the N-doped carbon materials show more favorable methanol tolerance and higher long-term stability than Pt/C (Fig. 4d and e).



**Fig. 4** (a) Preparation of the N-doped nanoporous carbon nanosheets from the *Typha orientalis* biomass; (b) SEM, TEM, and elemental mapping of the materials; (c) LSV curves of the materials in O<sub>2</sub>-saturated 0.1 M KOH solution; (d) LSV curves of the materials in O<sub>2</sub>-saturated 0.1 M KOH solution with and without 0.5 M of methanol; (e) chronoamperometric response of N-doped nanoporous carbon nanosheets and Pt/C electrodes at 0.10 V (vs. RHE) in O<sub>2</sub>-saturated 0.1 M KOH solution at a rotation rate of 800 rpm. (Reprinted with permission from ref. 153, Copyright 2015, RSC).

Due to its nontoxic and non-inflammable nature, urea should be a safer reagent to replace NH<sub>3</sub> for the introduction of nitrogen to the biochar matrix in practical applications. Urea can decompose to produce NH<sub>3</sub> at high temperature; therefore, the mechanism for the introduction of nitrogen into the biochar matrix by urea is similar to that by NH<sub>3</sub>. As an example, a porous nitrogen-doped carbon nanosheet (NCN) can be directly synthesized *via* the pyrolysis of cellulose and urea. The as-synthesized material

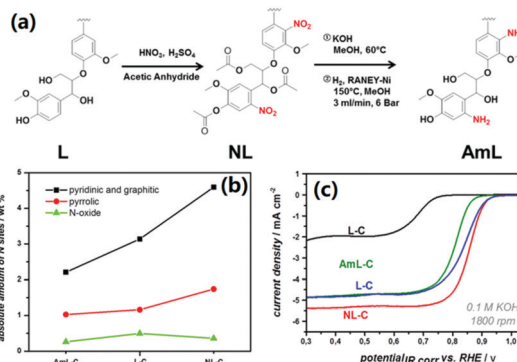


**Fig. 5** (a) Synthesis of the nitrogen-doped mesoporous biochar from beech wood lignin through an aromatic nitration process; (b) absolute abundance of nitrogen species in the nitrogen doped biochar materials produced from different lignin (calculated from XPS results); and (c) ORR performance of the biochar materials. (Reprinted with permission from ref. 155, Copyright 2016, American Chemical Society).

demonstrated excellent ORR catalytic performance with high electrocatalytic activity, better methanol tolerance and improved long-term durability compared with the commercial 20 wt% Pt/C catalyst. Notably, when urea is replaced by NH<sub>3</sub> gas during the pyrolysis process, the obtained nitrogen-doped biochar presented much poorer surface chemistry (lower graphitic/pyridinic N proportion) and porosity, resulting in bad ORR performance.<sup>154</sup>

Apart from NH<sub>3</sub> and urea treatments, which mainly introduce amino type nitrogen into biochar, the introduction of nitro type nitrogen should be another effective approach to preparing nitrogen-doped biochar materials. As shown in Fig. 5a, taking lignin (L) as an example, lignin was first subjected to a typical aromatic nitration process to obtain nitro-lignin (NL), which was further reduced into amino-lignin (AmL). The three as-synthesized types of lignin were then pyrolyzed with eutectic salt melt KCl/ZnCl<sub>2</sub> to obtain nitrogen-doped biochar materials. The biochar material obtained from NL shows a higher absolute abundance of quaternary and pyridinic-type nitrogen (Fig. 5b), leading to the best ORR performance<sup>155</sup> (Fig. 5c). Other recent studies of the applications of nitrogen-doped biochar materials for the ORR are summarized in Table 3.

Aside from N, the co-doping of additional heteroatoms, such as S, P, O, and B, into the carbon matrix of biochar could be another way to enhance the ORR performance due to synergistic effects. Gao *et al.*<sup>156</sup> reported the synthesis of N, S co-doped biochar with a porous 3D structure from honeysuckle biomass, and it includes a facile, slow pyrolysis and a conventional acid etching process. In addition to the well-doped N and S atoms, the as-synthesized materials also presented a 3D crosslinked network carbon structure with abundant macropores showing high ORR activity in 0.1 M KOH solution with superior tolerance to methanol and stability over the 20 wt% Pt/C catalyst. Such excellent ORR performance can be attributed to the synergistic effect, including a high number of ORR catalytic sites due to the S, N doping, favorable reactant transport channels provided by the pore structures, and the fast electron transfer rate induced by the continuous 3D networks.

Table 3 Summary of the applications of biochar-based materials for the ORR

Original biomass	Brief biochar synthesis methods	ORR activity (half-wave potential)	ORR activity (specific activity)	Ref.
Ginkgo leaf biomass	Pyrolysis of the Ginkgo leaf biomass in a tube furnace at 1100 °C for 5 h under Ar flow, then treated under flowing NH <sub>3</sub> at 1000 °C for 5 h	−0.154 V vs. Ag/AgCl	13.57 mA cm <sup>−2</sup> at −0.25 V vs. Ag/AgCl	2
Raw blood protein biomass	Carbonized the biomass at 350 °C under a N <sub>2</sub> atmosphere for 5 h, then heat-treated in flowing N <sub>2</sub> atmosphere at 1000 °C for 2 h	0.78 V vs. RHE	6.22 mA cm <sup>−2</sup> at 0.5 V vs. RHE	12
Catkin biomass	Pyrolysis of a mixture solution of catkins (400 mg), melamine (1 g), and FeCl <sub>3</sub> ·6H <sub>2</sub> O (200 mg) at 800 °C for 2 h	−0.194 V vs. Ag/AgCl	4.083 mA cm <sup>−2</sup> at −0.25 V vs. Ag/AgCl	18
Egg white biomass	Pyrolysis of a mixture solution of egg white biomass and FeCl <sub>3</sub> ·6H <sub>2</sub> O at 800 °C for 2 h	−0.130 V vs. Ag/AgCl	—	23
Water hyacinth biomass	Pyrolysis of a mixture solution of water hyacinth biomass and ZnCl <sub>2</sub> at 800 °C for 2 h	~0.83 V vs. RHE	4.083 mA cm <sup>−2</sup> at 0.4 V vs. RHE	29
Enoki mushroom (EM) biomass	The homogeneous EM powder was adequately mixed with cheap carbon nanotubes, then pyrolysis at 900 °C for 2 h	~0.81 V vs. RHE	~2.5 mA cm <sup>−2</sup> at 0.6 V vs. RHE	42
Willow and poplar catkin biomass	Carbonized the biomass at 550–950 °C under an Ar atmosphere for 60 min	−0.34 V vs. Ag/AgCl	—	47
Corn silk biomass	Hydrothermal carbonization of the biomass at 180 °C for 12 h, then annealed in an NH <sub>3</sub> atmosphere at 850 °C for 1 h, then mixed with FeCl <sub>3</sub> and annealed at 850 °C for 1 h	0.852 V vs. RHE	~2.0 mA cm <sup>−2</sup> at 0.6 V vs. RHE	57
Soybean biomass	Pyrolysis of a mixture solution of soybean biomass and ZnCl <sub>2</sub> at 900 °C	~−0.16 V vs. Ag/AgCl	~2.0 mA cm <sup>−2</sup> at −0.15 V vs. Ag/AgCl	59
Tapioca biomass	The tapioca biomass was mixed with silica, pre-carbonized in an Ar flow at 400 °C for 60 min, and then pyrolysis at 700 °C for 6 h under NH <sub>3</sub> flow	−0.20 V vs. Ag/AgCl	~1.0 mA cm <sup>−2</sup> at −0.2 V vs. Ag/AgCl	66
Coconut shell biomass	Pyrolysis of the coconut shells with H <sub>3</sub> PO <sub>4</sub> at 550 °C for 1 h, then carbonized with urea at 1000 °C for 2 h	−0.21 V vs. Ag/AgCl	5.3 mA cm <sup>−2</sup> at −0.8 V vs. Ag/AgCl	72
Eggplant biomass	Pyrolysis of the eggplant biomass with KOH in an Ar flow at 800 °C for 1 h, then carbonized at 1000 °C in an Ar flow (1.75 h) and NH <sub>3</sub> flow (0.25 h)	−0.336 V vs. Ag/AgCl	5.5 mA cm <sup>−2</sup> at −0.8 V vs. Ag/AgCl	75
Pomelo peel biomass	Pyrolysis of the mixture of pomelo peel biomass and melamine-cobalt nitrate at 800 °C in a N <sub>2</sub> flow for 1 h	−0.18 V vs. Ag/AgCl	5.2 mA cm <sup>−2</sup> at −0.8 V vs. Ag/AgCl	81
Nori ocean algae biomass	Hydrothermal carbonization of the mixture of algae biomass and melamine at 190 °C for 8 h, then annealed at 1000 °C for 1 h	−0.14 V vs. Ag/AgCl	5.8 mA cm <sup>−2</sup> at −0.8 V vs. Ag/AgCl	86
<i>Pulsatilla chinensis</i> Regel	Heated at 400 °C for 1 h, then carbonized at 700–1000 °C for 1 h	−0.137 V vs. Ag/AgCl	4.36 mA cm <sup>−2</sup> at −0.8 V vs. Ag/AgCl	88

Simultaneously introducing earth-abundant transition metals such as Fe, Ni, and Co into heteroatom-doped porous carbon is another effective approach to obtaining high-performance ORR catalysts.<sup>157</sup> An example is how iron-based, nitrogen-doped biochar materials (Fe–N–C) can be synthesized by the pyrolysis of a cheap and abundantly available soybean biomass precursor with the addition of metallic Fe.<sup>59</sup> The introduction of Fe into biomass during pyrolysis may facilitate the formation of planar pyridinic- and pyrrolic-N, both of which could provide active sites with enhanced ORR performance through a 4-electron transfer process. The nitrogen-doped biochar can also act as a catalyst support for improved ORR catalytic activity and durability because of the  $\pi$  bonding and the strong electron donor behavior of N atoms.<sup>158,159</sup> Pd nanoparticles supported on N-doped carbon from biomass have been reported to exhibit favorable electrochemical activity for the ORR with high catalytic performance and long-term stability.<sup>160</sup>

Although the biochar-based materials exhibited a comparable ORR performance with that of the benchmark 20 wt% Pt/C catalysts, the fuel cells using the biochar-based materials as cathode catalysts presented a significantly worse performance than the 20 wt% Pt/C cathode catalysts. However, it is still a promising alternative cathode catalyst for 20 wt% Pt/C in direct methanol fuel cells due to its high methanol tolerance.<sup>161</sup>

Furthermore, biochar-based materials can also act as cathode ORR catalysts for the air-breathing electrode in zinc–air batteries. Recent studies have indicated that a corn silk biomass derived N–P–Fe tri-doped carbon electrocatalyst showed excellent ORR activity and stability as well as high battery performance and specific capacity.<sup>57</sup> Very recently, biochar-based noble metal free ORR electrocatalysts have even demonstrated high energy efficiency and favorable stability in acidic polymer electrolyte membrane fuel cells (PEMFCs), a mainstream fuel cell technology.<sup>162</sup> With naturally abundant biomass resources, the new classes of noble metal-free, biochar-based ORR electrocatalysts can enable remarkable cost reduction without significant efficiency decrease, providing economic viability for fuel cell and other energy device (*e.g.*, metal–air batteries) applications.

### 3.2 Oxygen evolution reaction

The OER occurs in various energy conversion and storage technologies, such as water splitting and rechargeable metal–air batteries.<sup>146–148</sup> A four-electron process is involved in the OER, resulting in the sluggish nature and slow reaction kinetics of the OER. Therefore, high-performance catalysts are required to accelerate the OER and reduce the overpotential. Noble-metal oxides, such as IrO<sub>2</sub> and RuO<sub>2</sub>, are typical OER catalysts, showing high catalytic activity and favorable stability, but their high cost and scarcity greatly limit their commercialization.

Therefore, the development of alternative highly active and low-cost OER catalysts is critical for energy conversion and storage. Biochar, with its natural abundance and easily tuned surface chemistry and porous structure,<sup>77</sup> could be an ideal support loading non-noble active catalysts toward the OER. For instance, by the pyrolysis of widely available and renewable pomelo peel biomass with melamine, a nitrogen-doped porous biochar material with high surface area, abundant micropores and macropores, and a large amount of pyridinic/pyrrolic-N sites can be obtained and then integrated with ZIF-67, a cobalt-based metal-organic framework (MOF), to produce a biochar/ZIF-67 hybrid. The hybrid exhibited excellent OER catalytic performance in which the Co(III) species and Co-N structures made the main contribution; meanwhile, the strong interactions between ZIF-67 and the N-doped biochar were also favorable for the OER performance.<sup>163</sup>

Unlike conventional transition metal oxide-based OER catalysts, biochar-based materials often show favorable performance in both the OER and ORR. By the pyrolysis of melamine and cobaltous acetate with *Chlorella* biomass at 900 °C under an Ar atmosphere, a bamboo-like carbon nanotube-encapsulated Co NP was obtained (Fig. 6a and b), and it was then used as a bifunctional oxygen catalyst. Its ORR half-wave potential is 40 mV higher than that of a 20 wt% Pt/C catalyst (Fig. 6c); meanwhile, the OER overpotential at 10 mA cm<sup>-2</sup> is 23 mV lower than the reference IrO<sub>2</sub>/C catalyst in 1.0 M KOH solution (Fig. 6d). Such excellent bifunctional catalytic performance benefits mainly from the simultaneous increase in pyridinic N sites for the ORR and graphitic N sites for the OER in

the carbon matrix while the encapsulated Co nanoparticles can also improve the ORR and OER performance by creating new active catalytic sites.<sup>164</sup>

Apart from acting as a support for loading non-noble active catalysts, the biochar based material itself, taking advantage of easily realization of heteroatomic doping, can be used as a high performance OER electrocatalyst. As discussed above, biomass is rich in heteroatoms like nitrogen, sulfur and oxygen, making it a sustainable and cost-effective resource for heteroatomic doping in the resulting biochar based materials. An interesting result by Amiin *et al.*<sup>165</sup> is the report that sole-heteroatom-doped carbon materials derived from biomass without loading any metal species can also act as an efficient bifunctional oxygen catalyst. The researchers synthesized nitrogen (N) and sulfur (S) dual-doped 3D porous graphene from horn biomass through single-row pyrolysis, and the as-synthesized materials presented favorable performance in both the OER and ORR, comparable with the materials obtained through toxic chemicals and multistep routes.

Although the potential of biochar-based materials as oxygen electrocatalysts (ORR and OER) has been demonstrated, an important issue should be addressed. The evaluation of biochar-based electrocatalysts was based solely on half-cell measurements (3-electrode cell), whereas few reports have evaluated their performance *via* a full device such as zinc-air batteries. More future work should be devoted to the evaluation of membrane electrode assemblies (MEAs) such as the cathode and anode structure, ionomer interaction, gas-diffusion layers, membrane, and other interfering parameters. In this regard, a deeper understanding of the interaction of ionomers with the catalysts and the relationship between designing more active sites and long-term CO and methanol tolerance is crucially required for the practical application of biochar-based oxygen electrocatalysts.

## 4. Biochar-based materials for emerging fuel cells

Fuel cell technology, which provides high efficiency and relatively low greenhouse gas emissions, is one of the most effective solutions for the conversion of fossil fuels into electric energy.<sup>166,167</sup> The proton exchange membrane fuel cell (PEMFC) is the most widely used fuel cell technology, and it can convert the energy of chemical fuels (*e.g.*, H<sub>2</sub> and methanol) into electric energy. In PEMFCs, biochar-based materials mainly act as a cathodic ORR catalyst, which has been discussed in Section 3.1. Apart from PEMFCs, direct carbon fuel cells and microbial fuel cells are two burgeoning fuel cell technologies that can convert low-grade and dispersive energy into high-grade electric energy, and biochar-based materials can undertake new roles beyond that as a cathodic ORR catalyst in these two fuel cell technologies. A detailed discussion of these new roles is presented in the following sections.

### 4.1 Direct carbon fuel cells

Direct carbon fuel cells (DCFCs) have received considerable attention because they operate with the same electrochemical

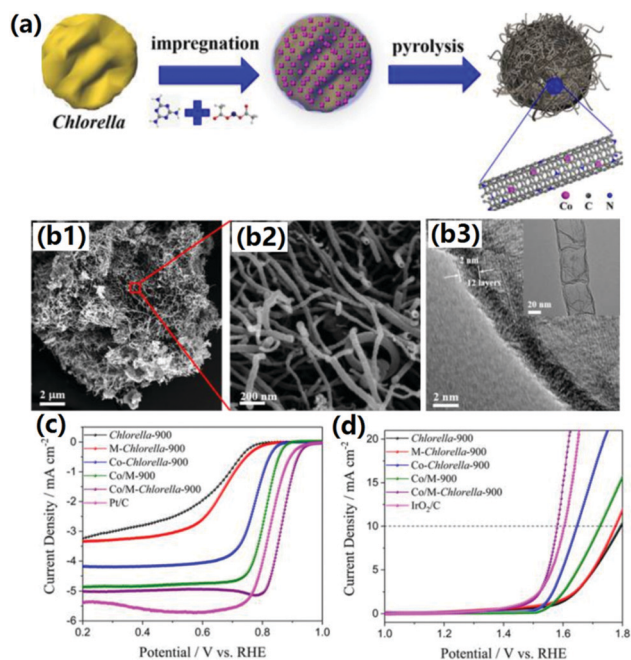


Fig. 6 (a) Schematic illustration of the synthesis of the bamboo like carbon nanotube encapsulated Co NPs from *Chlorella* biomass (named Co/M-Chlorella-900); (b1–b3) SEM and TEM images of the Co/M-Chlorella-900; (c) ORR performance; and (d) OER performance of the as-synthesized materials. (Reprinted with permission from ref. 164, Copyright 2017, American Chemical Society).

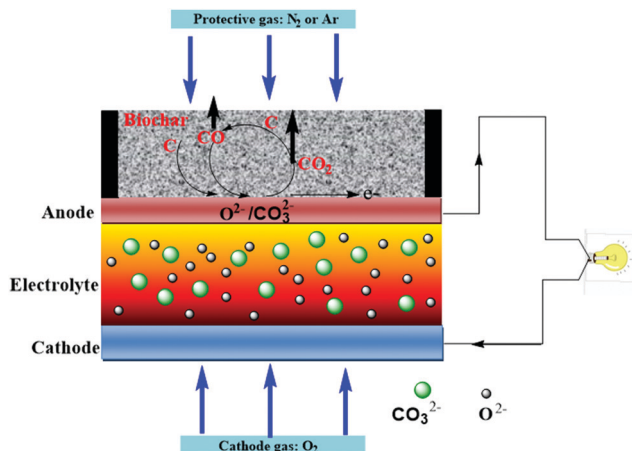


Fig. 7 A schematic diagram of a DCFC using biochar as the fuel and molten carbonate as the electrolyte.

principles as conventional fuel cells but directly convert the carbonaceous solid fuel into electricity in molten carbonate systems.<sup>168–170</sup> Potential sources for DCFCs including coal, coke, and activated carbon have been tested.<sup>171</sup> To achieve the goal of clean and efficient conversion of biomass into electricity, biochar can also be used as a DCFC fuel.<sup>172</sup> In typical operation of biochar-based DCFCs, molten carbonate is used as the electrolyte, which can contact well with the solid biochar fuel at high temperature, enhancing the diffusivity of the biochar to the reaction site. Meanwhile, it also provides high ionic conductivity and facilitates the diffusion and transportation of electrons. The carbon in the biochar is oxidized to CO<sub>2</sub> and CO on the anode, yielding many electrons that can move to the cathode and produce electricity (Fig. 7).

The physical properties of biochar materials, including crystallization and electrical conductivity, are reported to exert a great influence on the performance of DCFCs. Biochar materials with poorly crystallized, highly lattice disordered carbons are usually more reactive than conventional spectroscopic carbon and pyrolytic graphite in DCFCs due to the existence of more surface defects, such as edges and steps.<sup>173</sup> Thus, the DCFC performance could be enhanced. However, the poor crystallization may result in low electrical conductivity, which could increase the Ohmic polarization and restrict the carbon electrochemical reactions, thus lowering the DCFC performance.<sup>168</sup> Therefore, to improve the DCFC performance, it is important to find a balance between the crystallization and electrical conductivity of the biochar materials.

Apart from the crystallization and electrical conductivity, the texture features (surface area and pore size) and surface functional groups of biochar also play important roles in DCFCs. High surface area and pore volume can improve the interaction between biochar fuels and the molten carbonate electrolyte, thus improving the DCFC performance. The power density of DCFCs linearly increased with increasing mesopore content in the carbon fuels.<sup>174</sup> However, it is relatively insensitive to the micropore content, perhaps because the carbonate melt electrolyte could only partially access the micropores. The wettability of

carbon fuels by molten carbonate electrolytes is another factor affecting the performance of DCFCs. High wettability of carbon fuels could increase the accessibility for the electrochemical reaction and lower the Ohmic resistance, thus improving the DCFC performance. The power density could be enhanced by 30% when the carbon fuel was pre-soaked in the carbonate melt for several hours before cell functioning.<sup>175</sup>

In addition to the physical properties, the abundant surface functional groups and inorganic species of biochar fuel also have a significant influence on the DCFC performance. It has been demonstrated that increased surface oxygen functional groups can lead to enhanced DCFC performance.<sup>176,177</sup> Such enhancement may be due to the fact that the oxygen functional groups can provide more active sites for the chemisorption of O<sub>2</sub> molecules or O<sup>2-</sup> ions during cell operation.<sup>176</sup> Compared with conventional carbon fuel, biochar-based materials usually have more inorganic species,<sup>178</sup> which may affect the DCFC performance. Some elements may have negative impacts, while others could exhibit catalytic effects. The metal species that can be placed into inhibitive or catalytic categories were recently investigated,<sup>176,179</sup> and for DCFCs, MgO, CaO, and Fe<sub>2</sub>O<sub>3</sub> were found to act as catalysts for the carbon electrochemical process, while Al<sub>2</sub>O<sub>3</sub> and SiO<sub>2</sub> acted as inhibitors. In other work from the same group,<sup>180</sup> they found that the presence of inorganic species like K, Ni, and Ca could remarkably lower the carbon fuel gasification temperature by 200, 150, and 130 °C, respectively, to achieve the same power density output.

Understanding the effects of inorganic impurities on the performance is important for optimizing DCFCs when biochar-based materials are used as carbon fuels. From a thermodynamic view, biochar-based materials with high carbon content could deliver high power density, but the high ash content may lower the power output *via* limiting the mass flow from the fuel and reactive species to the electrodes, thus lowering the ionic conductivity.<sup>173</sup> However, as discussed above, some metal oxides like MgO, CaO, and Fe<sub>2</sub>O<sub>3</sub> could act as a catalyst for carbon oxidation in DCFCs, leading to an improvement of the power output of DCFCs.<sup>179</sup> Therefore, making a trade-off between the carbon content and inorganic impurities of biochar materials should be taken into consideration in optimizing biochar-based DCFCs.

Although biochar has a relatively low carbon content and a high ash content, the power density using biochar as fuel was 60–70% of that obtained using coal-based fuel cells.<sup>181</sup> This implies that biochar can possibly be used as a renewable, low-cost fuel for DCFCs. As reported by Elleuch and co-workers,<sup>166</sup> the peak power density delivered by almond shell biochar (127 mW cm<sup>-2</sup>) was much higher than that delivered by commercial activated carbon (100 mW cm<sup>-2</sup>). The cell performance can be maintained for a long time period due to the replenishment of oxygen-containing functional groups that continuously appear at the reactive edge of the biochar carbon matrix as the edge continuously advances. Furthermore, by adding an anode layer to a bi-layer pellet containing only the cathode and electrolyte, the cell performance and stability can be significantly improved; the peak power density

Table 4 Summary of the applications of biochar-based materials in DCFCs and MFCs

Original biomass	Biochar synthesis methods	Applications	Performance	Ref.
Wheat straw	Pyrolysis of the wheat straw biomass at 700 °C for 2 h, then loaded with Ca(NO <sub>3</sub> ) <sub>2</sub> and heat for another 2 h at 400 °C	DCFCs	Maximum power density: 258 mW cm <sup>-2</sup> ; open circuit potential: 0.98 V	7
Corn straw	Pyrolysis of the corn straw biomass at 700 °C for 1 h	DCFCs	Maximum power density: 218.5 mW cm <sup>-2</sup> ; open circuit potential: 1.06 V	14
Bamboo biomass	Pyrolysis of the bamboo biomass at 700 °C for 2 h	DCFCs	Maximum power density: 121 mW cm <sup>-2</sup> ; open circuit potential: 1.10 V	19
Pistachio shells	Pyrolysis of the pistachio shell biomass at 350 °C for 60 min	DCFCs	Maximum power density: 12.8 mW cm <sup>-2</sup> ; open circuit potential: 0.949 V	24
Corn cob	Pyrolysis of the corn cop biomass at 700 °C for 2 h, then loaded with Fe(NO <sub>3</sub> ) <sub>3</sub> and heat for another 1 h at 500 °C	DCFCs	Maximum power density: 270 mW cm <sup>-2</sup> ; open circuit potential: 1.0 V	30
Bamboo biomass	Pyrolysis of the bamboo biomass at 400 °C for 1 h, then activated with K <sub>2</sub> CO <sub>3</sub> at 800–1000 °C for 1–3 h	DCFCs	Maximum current density: 95.9 mA cm <sup>-2</sup>	43
Cellulose	Pyrolysis of the cellulose paper at 950 °C under NH <sub>3</sub> flow for 1 h	MFCs	Maximum power density: 1041 ± 90 mW m <sup>-2</sup> ; open circuit potential: 0.53 V	48
Pine wood	Pyrolysis of the pine wood biomass at 1000 °C for 1 h	MFCs	Maximum power density: 6 W m <sup>-2</sup> ; open circuit potential: ~0.72 V	56
Alfalfa leaf	Pyrolysis of the <i>Alfalfa</i> leaf biomass at 250 °C for 1 h, then activated with KOH, FeCl <sub>3</sub> , or ZnCl <sub>2</sub> at 900 °C for 2 h	MFCs	Maximum power density: 1328.9 mW m <sup>-2</sup> ; open circuit potential: 0.59 V	61
Yellow birch wood	Pyrolysis of the yellow birch wood 350–600 °C for 2–3 days	MFCs	Maximum power density: 11.11 mW m <sup>-2</sup> ; open circuit potential: 0.43 V	69
Corn cob	Pyrolysis of the corncob 250–700 °C for 2 h	MFCs	Maximum power density: 458.85 mW m <sup>-2</sup> ; open circuit potential: 0.221 V	74
Coconut shell	Pyrolysis of the H <sub>2</sub> SO <sub>4</sub> treated coconut shell biomass at 100–500 °C for 2 h	MFCs	Maximum current: 1.057 mA; open circuit potential: 0.722 V	79
Chitosan	Pyrolysis of the chitosan at 350 °C for 3 h, then treated with H <sub>3</sub> PO <sub>4</sub> and heated at 800–950 °C for another 3 h	MFCs	Maximum power density: 1603.6 ± 80 mW m <sup>-2</sup>	84

increases to 150 mW cm<sup>-2</sup>, and the stability period is improved to 130 min.<sup>182</sup> Table 4 summarizes recent studies on the applications of biochar-based materials for DCFCs.

Though biochar-based DCFC technology has experienced rapid development in the past few years, challenges in the fundamental and engineering aspects still exist. From the fundamental aspect, the mechanism for biochar electrochemical oxidation in different molten salt electrolytes and the dynamic behavior of biochar within the fuel–electrolyte interface should be further investigated to better understand the carbon electrochemical reaction at a molecular level. Understanding the underlying mechanism can provide useful information on developing efficient anode catalysts for DCFCs. Meanwhile, as almost all biochar materials contain heteroatoms like N, S, and P, and metal elements such as K, Na, Mg, Fe, and Ca, the impacts of these impurities on the carbon electrochemical oxidation rate, anode catalysts and current collector should be evaluated and the underlying mechanism should be elucidated. These results could provide useful information about to what extent biochar fuels need be pretreated before their feeding to DCFCs. From the engineering aspect, several practical challenges lie before the scale-up of DCFCs. Almost all the DCFCs investigated recently are essentially monopolar with a small electrode, and a large unit size and high IR drop are unavoidable when the DCFC is scaled up. Meanwhile, for a large-scale DCFC, the heat generated from the cell is usually insufficient to maintain the operating temperature. This problem can be solved *via* the integration of the DCFC with a molten carbonate fuel cell (MCFC) or solid oxide fuel cell (SOFC), but will significantly increase the operation costs. Considering these fundamental and engineering

challenges, there is a long way to go for the practical applications of biochar-based DCFCs.

#### 4.2 Microbial fuel cells

MFCs are another fuel cell technology that can convert the organic and inorganic contaminants and nutrients in wastewater to electricity through the metabolism of microorganisms.<sup>183,184</sup> Anode materials are important factors influencing the biofilm enrichment, internal resistance, and electron transfer rate from electroactive bacteria to the anode, thus determining the power generation and contaminant and nutrient conversion efficiency in MFCs.<sup>185</sup> The ideal cathodic catalysts applied in MFCs are required to have a high ORR catalytic activity and low costs, as MFCs are used mainly for wastewater treatment, and their capital and maintenance costs must be comparable to conventional wastewater treatment technologies. The energy produced by MFCs is primarily used to balance the energy consumption by wastewater treatment rather than to obtain additional economic benefits. Therefore, the properties associated with practicality, such as facile and large-scale synthesis, cost-effectiveness, and high durability should be considered preferentially when developing cathodic catalysts for MFCs. In this regard, biochar can be used as a promising cathodic catalyst for MFCs to replace granular activated carbon or graphite granules due to its low cost and easy scale-up synthesis, as well as high activity and durability. Moreover, the peak power output of a typical biochar-based MFC system is 532 ± 18 mW m<sup>-2</sup>, which is comparable with that of conventionally used granular activated carbon and granular graphite; however, the lower material expenses of biochar make the cost of its power output only 17 US\$ per W, which is much

cheaper than granular activated carbon (402 US\$ per W) or granular graphite (392 US\$ per W).<sup>186</sup>

Due to the rational porous structure and abundant surface functional groups, biochar has demonstrated favorable performance in MFCs. By the pyrolysis of cellulose using ammonium phosphate as a doping source, Liu and co-workers<sup>187</sup> prepared a nitrogen and phosphorus dual-doped biochar and used it as a high-performance oxygen reduction catalyst for MFCs. The air cathode using the dual-doped biochar catalyst achieved a maximum power density of  $2293 \pm 50 \text{ mW m}^{-2}$ , which is significantly higher than that obtained using a Pt/C catalyst ( $1680 \pm 32 \text{ mW m}^{-2}$ ). An air cathode was built with a catalytic layer comprising biochar for MFCs.<sup>188</sup> A maximum power density of  $500 \pm 17 \text{ mW m}^{-2}$ , comparable with that of the Pt cathode, was obtained from the biochar produced by the pyrolysis of sewage sludge at  $900 \text{ }^\circ\text{C}$ . More importantly, the as-prepared cathode catalytic layer exhibited good stability and great tolerance to methanol: with more than two months of operation under  $1 \text{ k}\Omega$  external loading, there was little voltage change in the biochar-coated cathode of the MFC; with a sudden increase in methanol concentration in the MFC system, the current in the biochar-coated cathode remained nearly unchanged. These results suggest that the biochar-coated cathode created less of a crossover effect, which may extend the applications of biochar as an ORR catalyst to other fuel cell systems. More recent investigations into the applications of biochar-based materials for MFCs can be found in Table 4.

Although biochar has shown excellent performance when acting as a cathodic catalyst in MFCs, biofouling on biochar cathodes should be taken into account, as it would deteriorate the MFC performance remarkably if not properly treated. For example, the performance of bamboo biochar cathodes in the presence of biofilms showed decreases in power density by 11.8% and 21.6% at  $0.1 \text{ V}$  and  $0 \text{ V}$ , respectively, after 2-month operation of the MFC. When the biofilm was eliminated from the biochar cathodes, the power density of the MFC could be slightly recovered.<sup>189</sup> To avoid biofouling, an effective approach was to modify the biochar cathode with a disinfectant quaternary ammonium compound to inhibit biofilm growth. The biofilm on the modified cathode was 26 times less than that on the control electrode even after 2-month operation. After 5-month operation, the maximum power density of the modified cathode decreased by only 1–7%. For comparison, the power density of the benchmark Pt/C catalyst retained only 21% of its initial value at the same time.<sup>190,191</sup>

In the past few years, great efforts have been made to modify biochar-based cathodic catalysts to improve MFC performance and long term stability to meet the requirements of scale-up applications. However, several problems still remain in this area. First, the biochar itself usually has favorable biocompatibility, but many methods for biochar modification, *e.g.*, surface doping with heteroatoms like N, S, or P and surface recombination with metal or metal oxide nanostructures, will reduce its biocompatibility. This may deteriorate the MFC performance due to the suppression of electroactive bacteria growth on the electrode. Thus, a balance between improving

the ORR catalytic activity and reducing the biocompatibility should be taken into account in future work on biochar modifications for MFC cathodic catalysts. Second, the underlying mechanism of how the modified biochar materials improve the MFC performance is not yet elucidated. How to rationally design an efficient cathodic catalyst with high performance and stability based on understanding such a mechanism is still a challenge.

## 5. Biochar-based materials for supercapacitors

Supercapacitors, also known as double-layer electrochemical capacitors (EDLCs), offer a promising approach for the storage of clean and renewable energy and have attracted considerable attention due to their long cycle-life, high power and energy density, and superior reversibility.<sup>192</sup> As mentioned above, compared with conventional carbon materials, raw biochar materials are often abundant in oxygenated functional groups, *e.g.*, OH, C=O, and COOH, and the oxygen content can be tuned through the pyrolysis conditions, *e.g.*, temperature and heating rate. In addition, by selecting the proper biomass precursor, pyrolysis conditions, and catalyst, other functionalities that may greatly enhance the pseudo-capacitance performance and increase the amount of energy stored in the supercapacitor can be introduced into the final biochar material. Furthermore, some electrochemically inert oxygenated functional groups can improve the wettability of the carbon electrode and, consequently, enhance the specific capacitance by improving pore access and increasing surface utilization.<sup>121</sup> In addition, high contents of oxygenated functional groups can prevent further oxidation of the carbon matrix under a wide range of potentials,<sup>193</sup> greatly enhancing the cycle stability of the electrode materials. Through single-step pyrolysis of plant leaves at  $1000 \text{ }^\circ\text{C}$ , a functional microporous conducting biochar material with a high surface area of approximately  $1230 \text{ m}^2 \text{ g}^{-1}$  was directly synthesized.<sup>97</sup> The concurrent high conductivity and microporosity of biochar-based materials are key to high-performance supercapacitor applications, and the as-synthesized material indeed showed a very high specific capacitance of  $400 \text{ F g}^{-1}$  with an energy density of  $55 \text{ W h kg}^{-1}$ . However, as demonstrated previously,<sup>194</sup> some high-polarity oxygen groups including carboxyl, anhydride, and lactone may hinder the diffusion of electrolyte ions, increasing the resistance and causing capacitance fading at high current densities. Even worse, as described previously, some raw biochars possess limited developed porosity and very small surface area, greatly decreasing their EDLC performance. This limitation has recently been circumvented by different activations that can endow biochar with a high surface area and porosity, as reviewed in our previous work.<sup>77</sup>

As mentioned previously, KOH activation allows control over the pore size distribution and increases the surface area of biochars. Bamboo-derived biochar was activated using different ratios of KOH to biochar (KOH:biochar),<sup>195</sup> and the nitrogen adsorption-desorption isotherms showed that micropore development was nearly complete when KOH:biochar = 2;

the further addition of KOH resulted in the formation of larger pores. As the KOH : biochar ratio was increased from 1 to 4, the BET surface area increased from 1010 to 1400 m<sup>2</sup> g<sup>-1</sup>, the total pore volume increased from 0.123 to 0.708 cm<sup>3</sup> g<sup>-1</sup>, and the micropore percentage increased from 67.6% to 88.7%. Using an aqueous electrolyte (30 wt% H<sub>2</sub>SO<sub>4</sub>), the activated biochar with a relatively high mesopore fraction had a higher capacitance in the high discharge current density region (300–800 mA cm<sup>-2</sup>). Similar results were also found when a non-aqueous electrolyte (1 M of tetraethylammonium tetrafluoroborate (Et<sub>4</sub>N-BF<sub>4</sub>)) was used with a larger ionic radius (0.74 nm for Et<sub>4</sub>N<sup>+</sup>) in an aprotic propylene carbonate solvent. This phenomenon can be explained by the fact that larger mesopores can facilitate ion transfer and diffusion while smaller micropores can hinder the transfer and diffusion of ions, thus decreasing the capacitance of the material. A similar phenomenon has been observed when conventional activated carbon was used as the supercapacitor electrode material.<sup>196</sup>

By impregnating cherry stone biomass with different activating agents such as H<sub>3</sub>PO<sub>4</sub>, ZnCl<sub>2</sub>, and KOH solutions and heating it in N<sub>2</sub> at temperatures between 400 and 900 °C, a series of activated biochar materials were prepared.<sup>197</sup> KOH activation at 800–900 °C led to porous biochars with large specific surface areas between 1100 and 1300 m<sup>2</sup> g<sup>-1</sup> and average pore sizes of approximately 0.9–1.3 nm. This textural feature allows the electrolyte ions to more easily access the porous network. At a low current density, a maximum capacitance of 230 F g<sup>-1</sup> in 2 M H<sub>2</sub>SO<sub>4</sub> aqueous electrolyte and 120 F g<sup>-1</sup> in 1 M (C<sub>2</sub>H<sub>5</sub>)<sub>4</sub>NBF<sub>4</sub>/acetonitrile aprotic medium could be achieved. More importantly, this high capacitance performance could be maintained when the current density was increased.

In addition to tuning the pore structure and surface area, introduction of heteroatoms into the carbon matrix of the biochar material is another effective approach to improving the capacitance performance. The heteroatom most commonly used to cause faradaic pseudocapacitive reactions in carbon materials is nitrogen, and nitrogen-doped biochar materials are extensively used as supercapacitor electrode materials. The capacitance performance of a nitrogen-containing biochar material (carbonized eggshell membrane, CEM) activated with KOH (Fig. 8a) has been studied by Li *et al.*, recently,<sup>198</sup> and the results show that although the as-synthesized material had a relatively low surface area of 221 m<sup>2</sup> g<sup>-1</sup>, it could achieve exceptional specific capacitances of 297 and 284 F g<sup>-1</sup> in basic and acidic electrolytes, respectively, in a three-electrode system (Fig. 8c). These values are much higher than that of conventional activated carbon with a high surface area and pore volume (203 F g<sup>-1</sup>). This superior capacitance is mainly attributed to the pseudocapacitance arising from the redox reactions of the nitrogen and oxygen functionalities (the material contained 10 wt% oxygen and 8 wt% nitrogen) (Fig. 8b). Pyridinic and pyrrolic nitrogen species accompanied by a quinone oxygen group, a negatively charged group located at the edges of the biochar carbon matrix, have been reported to contribute mainly to the capacitance,<sup>199</sup> while the quaternary and pyridinic N species can enhance the electron transport and introduce pseudocapacitance

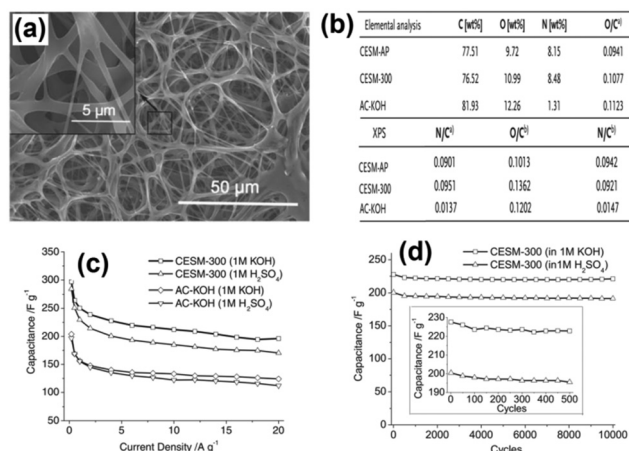


Fig. 8 (a) The SEM images of the carbonized eggshell membrane activated with KOH (CESM-300); (b) the elemental composition of the as-prepared CEM and activated CEM; (c) gravimetric capacitances measured at various charge/discharge current densities for the CESM-300 and KOH activated carbon without N doping; and (d) long-term cycle performance of the CESM-300 at a current density of 4 A g<sup>-1</sup>. Reprinted with permission from ref. 198. Copyright 2012, Wiley-VCH Verlag GmbH & Co. KGaA, Weinheim.

by interacting with protons in acid electrolytes, thus also enhancing the EDLC capacitance.<sup>200</sup> Furthermore, the electrodes demonstrated excellent cycling stability; only 3% capacitance fading was observed after 10 000 cycles, demonstrating good conductivity and rapid charge propagation in both acidic and basic electrolytes (Fig. 8d).

The pseudocapacitance caused by phosphorus-containing groups in activated biochar materials has also been investigated. Hulicova-Jurcakova and co-workers<sup>202</sup> first reported the introduction of phosphorus-containing functional groups into the carbon matrix of biochar derived from fruit stones *via* the activation of phosphoric acid in pyrolysis. The phosphorus-rich porous biochar with a surface area of 1055 m<sup>2</sup> g<sup>-1</sup> and a phosphorus content of 8.52 wt% was used as a supercapacitor electrode material. It could be stably operated at voltages larger than 1.3 V in aqueous H<sub>2</sub>SO<sub>4</sub>, and it has a specific capacitance of 192 F g<sup>-1</sup> and a very long cycle life (15 000 cycles). Phosphorus was confirmed to strongly facilitate the pseudocapacitance and enhance the stability. Subsequently, several phosphorus-rich biochar-based materials have been synthesized and used for supercapacitors; the most remarkable observation resulting from these studies was that phosphorus-rich biochar-based electrode materials increased the range of tolerated voltage.<sup>203,204</sup>

Apart from the doping of heteroatoms in the carbon matrix, another approach to introducing pseudocapacitance into supercapacitors is to load electroactive species such as metal oxides onto the carbon surface. A simple, scalable, cost-effective, and green approach has been developed to fabricate a binder-free asymmetric supercapacitor using bacterial cellulose-derived CNFs loaded with MnO<sub>2</sub> as the electrode materials.<sup>205</sup> The as-synthesized materials can be reversibly charged/discharged at an operation voltage of 2.0 V in 1.0 M Na<sub>2</sub>SO<sub>4</sub> aqueous electrolyte, delivering a high energy density of 32.91 W h kg<sup>-1</sup> and a maximum power density of 284.63 kW kg<sup>-1</sup> while retaining 95.4% of the

Table 5 Summary of biochar based electrodes for supercapacitors through pyrolysis, and hydrothermal treatment coupled with activation

Original biomass	Synthesis of biochar	Surface area (m <sup>2</sup> g <sup>-1</sup> )	Electrolyte	Current density (A g <sup>-1</sup> )	Specific capacitance (F g <sup>-1</sup> )	Ref.
Gelatin	Pyrolysis of gelatin at 600 °C, then activated the biochar at 800 °C with KOH (1:2) for 1 h	2774	KOH (6 M)	0.5	~300	9
Silk	Pyrolysis of silk with KOH (100:16) at 800 °C for 3 h	2557	H <sub>2</sub> SO <sub>4</sub> (1 M)	0.1	264	15
Elm samara	Pyrolysis of dry <i>Elm samara</i> with KOH (5 g to 50 mL 8 M KOH solution) at 700 °C for 2 h	1947	KOH (6 M)	1	470	21
Bamboo	Hydrothermal treatment of bamboo at 200 °C for 12 h to obtain hydrochar, then activated the hydrochar with KOH (1:1) at 800 °C for 1 h	1472	KOH (6 M)	0.1	301	27
Hemp stems	Pyrolysis of the hemp stems at 600 °C for 2 h, then activated at 800 °C with steam (2.0 mL-H <sub>2</sub> O (g-char h) <sup>-1</sup> ) for 2 h, then loading with MnO <sub>2</sub>	438	Na <sub>2</sub> SO <sub>4</sub> (1 M)	1	340	41
Watermelon	Hydrothermal treatment of watermelon at 180 °C for 12 h, then activated the hydrochar with FeCl <sub>3</sub> and FeSO <sub>4</sub> at 550 °C for 4 h	—	KOH (6 M)	0.5	358	46
Bagasse	Pyrolysis of the mixture of bagasse, CaCl <sub>2</sub> and urea at 800 °C for 2 h	946	KOH (6 M)	1	323	55
Soybean roots	Pyrolysis of the soybean roots at 500 °C for 2 h, then activated the biochar with KOH (1:4.5) at 800 °C for 2 h	2143	KOH (6 M)	0.5	276	62
<i>Aloe vera</i>	Pyrolysis of the <i>Aloe vera</i> at 400 °C for 3 h, then activated the biochar with KOH (1:3) at 800 °C for 2 h	1890	H <sub>2</sub> SO <sub>4</sub> (1 M)	0.5	410	67
Almond shells	Pyrolysis of the almond shell at 700–900 °C for 4 h, then activated the biochar with KOH (1:4) at 800 °C for 2 h	1363	KOH (6 M)	1	286	73
Hemp	Hydrothermal treatment of hemp bast fiber at 180 °C for 24 h, then activated the biochar with KOH (1:1) at 800 °C for 1 h	2287	KOH (6 M)	1	122	78
Sawdust	Pyrolysis of the mixture of sawdust with FeCl <sub>3</sub> (1 mM g <sup>-1</sup> ) at 800 °C for 1 h	421	K <sub>2</sub> SO <sub>4</sub> (0.5 M)	0.5	128	83
<i>Typha angustifolia</i>	Fast pyrolysis of the <i>Typha angustifolia</i> at 500 °C, then activated the biochar with KOH (1:4) at 800 °C for 2 h	3062	K <sub>2</sub> SO <sub>4</sub> (0.5 M)	0.5	257	87
Bamboo	Fast pyrolysis of the mixture of bamboo biomass with K <sub>2</sub> FeO <sub>4</sub> , at 800 °C for 2 h	1732	KOH (6 M)	0.5	222	93
Seaweed	Direct pyrolysis of the seaweed at 600–900 °C for 3 h	3487	H <sub>2</sub> SO <sub>4</sub> (1 M)	0.05	203	94
Neem leaves	Direct pyrolysis of the neem leaves at 600–1000 °C for 5 h	1230	H <sub>2</sub> SO <sub>4</sub> (1 M)	0.5	400	77 and 97

capacity after 2000 cycles. Other recent studies on biochar-based materials for supercapacitor applications are summarized in Table 5.

Recent studies show that various biochar-based materials with supercapacitor properties comparable with those of commercial activated carbon materials can be produced using simple pyrolysis/hydrothermal treatment coupled with activation approaches. However, to find applications of biochar-based functional materials in practical supercapacitors, the following challenges and issues should be addressed. First, due to the diversity of biomass, fundamental studies should focus on the influence of the biomass composition on the capacitive performance of the resulting biochar-based materials. Conducting these investigations with lignin-, cellulose-, and hemicellulose-derived biochar materials could be a good choice. Second, hierarchical porous biochar materials with high specific surface areas and controllable pore size, pore geometry, and pore connection can be easily produced using the chemical (*e.g.*, KOH, H<sub>3</sub>PO<sub>4</sub>, and ZnCl<sub>2</sub>) activation method. Furthermore, the conventional chemical activation method is usually unfavorable for creating graphitic carbon structure in biochar materials because it may suppress their electrical conductivity and surface wettability towards an electrolyte. Chemical activation in combination with heteroatom- (*e.g.*, N, S, P, and O) doping or nanostructure recombination may enable the preparation of biochar-based materials with an appropriate pore structure, good electrical conductivity, and

good wettability towards electrolytes. Third, most of the state-of-the-art biochar-based electrode materials with excellent capacitive performance were recently produced at a lab scale. Future work should be devoted to developing a process protocol to scale up the production of biochar-based electrode materials. Fourth, a new research area can be explored to prepare biochar fibers and foams to construct electrodes for flexible supercapacitor devices with the advantages of portability and flexibility for applications in future portable electronics. Finally, the energy density of supercapacitors can be increased by increasing the pseudocapacitance or widening the operation voltage. Introducing pseudocapacitive materials, such as heteroatoms, metal oxides, or conductive polymers, to biochar-based materials should be a future focus to increase the capacitance. Widening the voltage window by replacing the aqueous electrolytes with ionic liquids as electrolytes or fabricating hybrid capacitors should be another effective way to improve both the energy density and power density of biochar-based supercapacitors.

## 6. Biochar-based materials for lithium/sodium batteries

Due to its high energy/power density and high energy efficiency, the rechargeable Li<sup>+</sup> ion battery (LIB) is one of the most

successfully commercialized electrochemical storage devices, with its applications extending from portable devices to electric vehicles.<sup>206–208</sup> Because ion diffusion plays a critical role in the charge/discharge processes, and a large surface area might not be beneficial for LIBs from the safety point of view and the perspective of irreversible losses in the formation cycles,<sup>209</sup> biochar-based materials with a moderate surface area and unique structural characteristics (*e.g.*, versatile pore structure, abundant surface functional groups, and various inorganic species) are highly desired for LIBs to enhance the diffusion of  $\text{Li}^+$  and provide a large interface of the electrode/electrolyte, thus benefiting the electrochemical reactions in LIBs.<sup>106,210,211</sup> Meanwhile, there are other two reasons why biochar can be considered as efficient anode components in LIBs. First, biochar-based materials can be synthesized *via* cost-effective and sustainable approaches. Second, their specific capacity is much higher than that of conventional graphite materials. For example, interconnected highly graphitic carbon nanosheets (HGCNS) were synthesized from wheat stalk biomass by combined hydrothermal and graphitization processes.<sup>212</sup> The as-synthesized HGCNS showed a unique interconnected two-dimensional (2D) nanostructure with a thickness of 1.0–2.0 nm, which corresponds to about 2–6 single graphene layers. Such 2D nanostructure could not only provide multiple  $\text{Li}^+$  storage sites, but also facilitate rapid electron and  $\text{Li}^+$  ion transport. Meanwhile, the HGCNS showed a very high graphitization degree, which can bring about a low and flat charge–discharge voltage plateau, thus greatly reducing the voltage hysteresis. As an anode material in LIBs, the as-prepared HGCNS delivered a reversible capacity of  $502 \text{ mA h g}^{-1}$ , 1.35 times higher than the theoretical capacity of graphite, as well as excellent rate capability and superior cycling performance. Jiang *et al.*<sup>201</sup> recycled waste bamboo cellulose fibers and then treated them with a controllable hydrothermal process conducted in an alkaline solution to obtain uniform carbon fibers (Fig. 9a and b). The bamboo-based carbon fibers delivered a high reversible capacity of  $710 \text{ mA h g}^{-1}$ , which can be maintained without decay in up to

300 cycles with a coulombic efficiency of almost 100% (Fig. 9c). In addition to increasing the surface area and improving the conductivity of the electrode material, the porous structure also provides fast ion diffusion channels, thus contributing to higher lithium storage capacity. Therefore, further work should be devoted to improving the synthesis of porous biochar with uniform porosity and a high surface area.

Apart from a porous structure and high surface area, doping electron-rich N atoms into the graphite carbon matrix of biochar would also introduce more chemically active defects, thus not only enhancing the electronic conductivity but also providing more available active sites for  $\text{Li}^+$  adsorption, resulting in high  $\text{Li}^+$  storage capacity.<sup>213,214</sup> The hybridization between the lone pair of electrons in N atoms and the p-electrons in C atoms can make the neighboring carbons atoms in the biochar matrix more electronegative, thus providing more active sites for  $\text{Li}^+$  storage. Chen *et al.*<sup>3</sup> prepared hierarchically porous N-rich biochar materials from wheat straw, with a N content of 5.13 wt%. The as-synthesized biochar material contains more pyridinic N (N-6) and pyrrolic-N (N-5) than oxidized N (N-X) and quaternary N (N-Q) (Fig. 10a), which is a critical factor for its high reversible  $\text{Li}^+$  storage capacity because, based on the theoretical calculations, N-5 and N-6 are more favorable than N-X and N-Q for  $\text{Li}^+$  storage.<sup>215,216</sup> When used as an anode for Li-ion batteries, the as-synthesized biochar material exhibits a superior specific capacity of  $1470 \text{ mA h g}^{-1}$  at  $37 \text{ mA g}^{-1}$  and possesses an ultra-high rate capability of  $344 \text{ mA h g}^{-1}$  at  $18.5 \text{ A g}^{-1}$ . The reversible capacity remains as high as  $198 \text{ mA h g}^{-1}$  even at an extremely high current density of  $37 \text{ A g}^{-1}$  (Fig. 10b). The cycling performance of the biochar material is also very impressive. As shown in Fig. 10c, when tested at  $0.37 \text{ A g}^{-1}$  and  $3.7 \text{ A g}^{-1}$ , the reversible capacity remains at  $976 \text{ mA h g}^{-1}$  and  $659 \text{ mA h g}^{-1}$ , respectively, even after 300 cycles. As proposed by the authors, the reasons for the excellent cycle performance and high specific capacity of the material can be concluded as follows: first, as shown in Fig. 10d, the hierarchically porous structure of biochar-based materials not only offers a large electrode/electrolyte interface for the charge transfer reaction but also provides abundant functional pores with various dimensions for  $\text{Li}^+$  storage; second, a high inherent N content may allow strong electronegativity and interactions between the biochar matrix and  $\text{Li}^+$ , thus enhancing the electronic conductivity and electrochemical stability; and third, the presence of thinner walls and interconnected pores decreases the inner resistance, shortening the  $\text{Li}^+$  diffusion pathway. This work may present some important scientific insights into the design and preparation of metal-free anode materials with high rates from renewable biomass resources.

Compositions comprising biochar and transition metal oxides have also widely been used as LIB electrodes. Transition metal oxides, such as  $\text{Co}_3\text{O}_4$ ,<sup>219</sup>  $\text{Fe}_3\text{O}_4$ ,<sup>220</sup> and  $\text{MnO}_2$ ,<sup>221</sup> were used as anode materials for LIBs due to their remarkably higher specific capacities than that of commercial graphite. However, the practical application of transition metal oxides in LIBs is restricted by their large volume expansion–contraction and severe particle aggregation, causing electrode pulverization, capacity loss or poor cycling stability.<sup>218</sup> The combination of

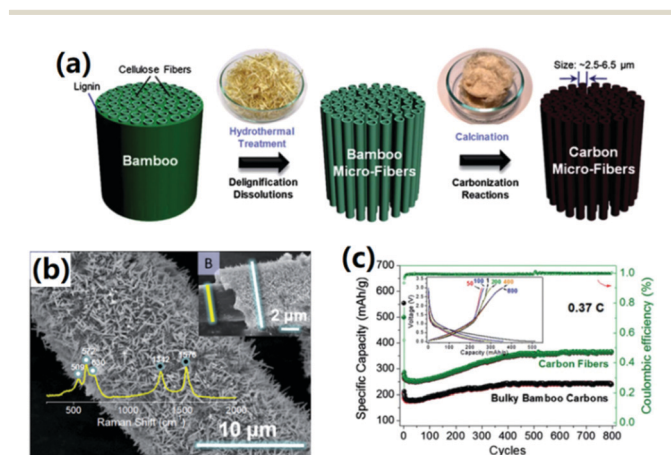


Fig. 9 (a) Schematic diagram displaying the overall evolution of bamboo chopsticks into uniform carbon fibers; (b) SEM image of the carbon fibers and (c) long-term cyclic performance and charge–discharge profiles. (Reprinted with permission from ref. 201. Copyright 2014, Royal Society of Chemistry).

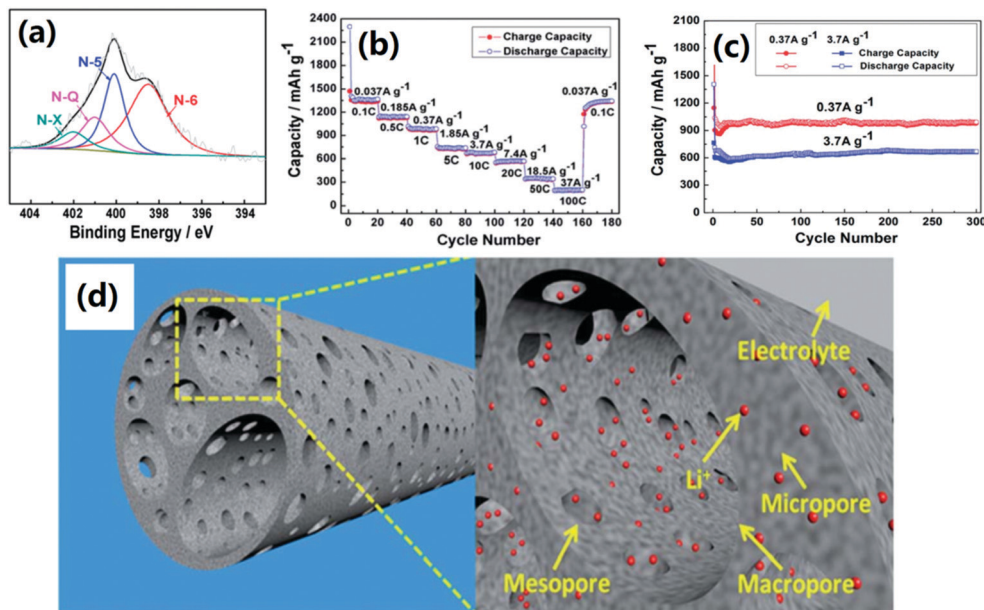


Fig. 10 (a) XPS N 1s spectrum of the hierarchically porous N-rich biochar materials; (b) The capacity of the hierarchically porous N-rich biochar materials over cycling at different rates; (c) cycling performance of the hierarchically porous N-rich biochar materials at 3.7 and 37 A g<sup>-1</sup>; and (d) schematic mechanism of the hierarchically porous structure and Li-ion storage in the hierarchically porous N-rich biochar materials. (Reprinted with permission from ref. 3, Copyright 2014, Royal Society of Chemistry).

metal oxides with porous biochar materials should be an effective approach to overcoming these limitations because of the high electronic conductivity, good corrosion resistance and series of favorable surface properties of the carbon materials.<sup>222,223</sup> Cheng *et al.*<sup>217</sup> employed *Auricularia* biomass as the retractable support to synthesize an interconnected MnO@biochar hybrid nanoflake network (MFC-1, Fig. 11a). When evaluated as an anode material for LIBs, MFC-1 delivered a reversible capacity of 868 mA h g<sup>-1</sup> at 0.2 A g<sup>-1</sup> over 300 cycles and 668 mA h g<sup>-1</sup> at 1 A g<sup>-1</sup> over 500 cycles, with a coulombic efficiency of almost 100% (Fig. 11b and c), indicating a superior cycle stability and a high Li<sup>+</sup> storage capacity. Wang *et al.*<sup>218</sup> developed a simple and industrially scalable approach to prepare porous biochar materials with abundant nitrogen and high surface areas from crawfish shell biomass and then used the porous biochar materials as supporting materials to synthesize N-doped porous carbon/Co<sub>3</sub>O<sub>4</sub> nanocomposites (Fig. 12a). The resulting material was employed as an anode material for LIBs, which released an initial discharge of 1223 mA h g<sup>-1</sup> at a current density of 100 mA g<sup>-1</sup> and still maintained a high reversible capacity of 1060 mA h g<sup>-1</sup> after 100 cycles, which is much higher than those of individual N-doped porous carbon (PC) or Co<sub>3</sub>O<sub>4</sub> (Fig. 12b).

The rechargeable lithium-sulfur battery (LSB) is an emerging lithium battery with a much higher theoretical specific capacity (1675 mA h g<sup>-1</sup>) and specific energy (2600 W h kg<sup>-1</sup>) compared with those of conventional LIBs.<sup>224-228</sup> Carbon-based materials, with rational pore features, high surface area, satisfactory electrical conductivity, and abundant frameworks, could be efficient sulfur hosting materials for LSB cathodes.<sup>229,230</sup> In the lithiation-delithiation process, the carbon matrix could encapsulate sulfur and trap polysulfides, thus suppressing the

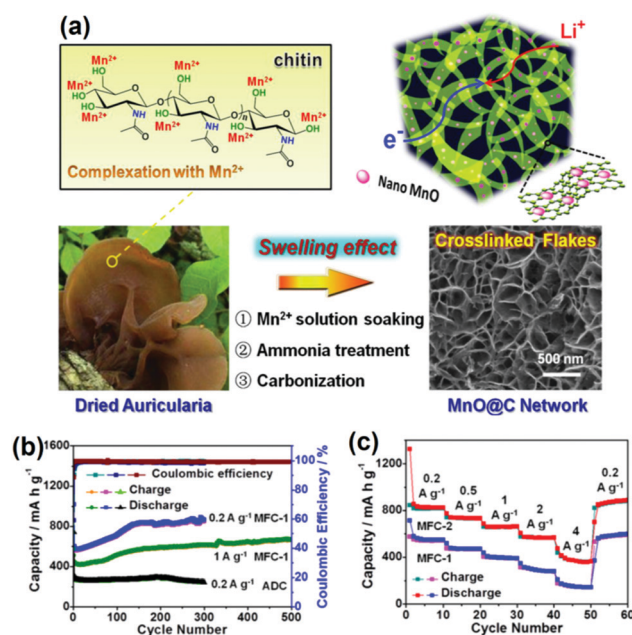


Fig. 11 (a) Schematic illustration of the synthesis of the MnO@biochar nanoflake network; (b) cycling performance of the MnO@biochar hybrid (MFC-1) and the pure carbon (ADC) obtained from pyrolysis of auricularia; and (c) rate capabilities of the MnO@biochar hybrids cycled 10 times at each current density. (Reprinted with permission from ref. 217. Copyright 2016, American Chemical Society).

active material volume expansion and enhancing the long-term stability of the LSB.<sup>231</sup>

Effective encapsulation of sulfur and enhanced conductivity should be taken into account first in the design of carbon/

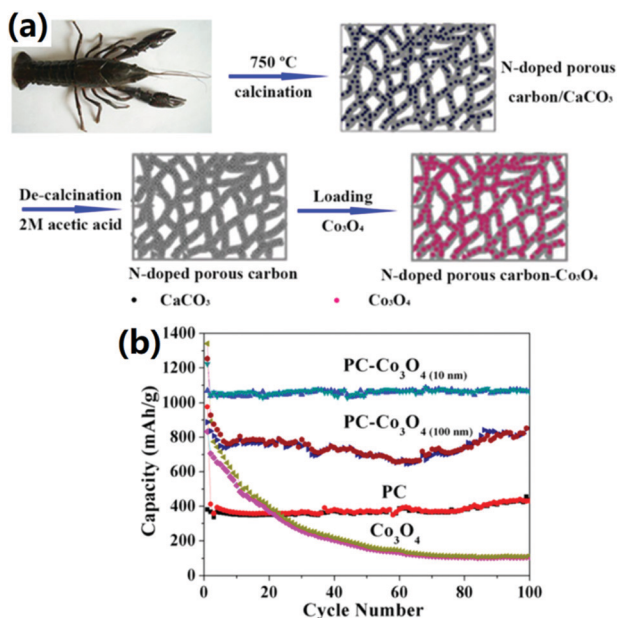


Fig. 12 (a) Fabrication process of the crawfish shell-derived PC- $\text{Co}_3\text{O}_4$  nanocomposites; and (b) cycling performance of the N-doped PC,  $\text{Co}_3\text{O}_4$ , N-doped PC- $\text{Co}_3\text{O}_4$  (100 nm), and N-doped PC- $\text{Co}_3\text{O}_4$  (10 nm) nanocomposites at a current density of  $100 \text{ mA g}^{-1}$ . (Reprinted with permission from ref. 218, Copyright 2014, American Chemical Society).

sulfur composite cathodes for LSBs.<sup>232,233</sup> For this purpose, sufficient space in the carbon matrix is necessary for sulfur encapsulation, polysulfide trapping and volume change suppression. Also, suitable contact areas with the electrolyte are necessary for the electrode reaction.<sup>234</sup> Biochar should be a promising candidate satisfying the above criteria because of the following reasons: firstly, the highly porous structure of biochar can hold a sufficient amount of sulfur without decreasing the buffering space for possible volume expansion. Secondly, the well graphitized carbon matrix endows biochar with a high conductivity, which could facilitate the sulfide shuttle process. Finally, the pore size and distribution of biochar can be rationally tuned to synthesize sulfur arrays with desired dimensions.<sup>105,106</sup>

Due to the above advantages, various biochar materials derived from different biomass have been used as efficient sulfur hosting materials for LSB cathodes. Qu *et al.*<sup>6</sup> prepared a highly ordered nitrogen-rich mesoporous biochar *via* pyrolysis of zeolite templated gelatin biomass (Fig. 13a). This biochar material had a rod like morphology, a high surface area and mesopore structure, and abundant nitrogen content (Fig. 13b-f). It could hold 53.3 wt% sulfur homogeneously inside the mesopores, and the obtained sulfur-biochar composite presented a high rate capability and long-term cycling stability as LSB cathode materials (Fig. 13g-j). Such excellent performance of

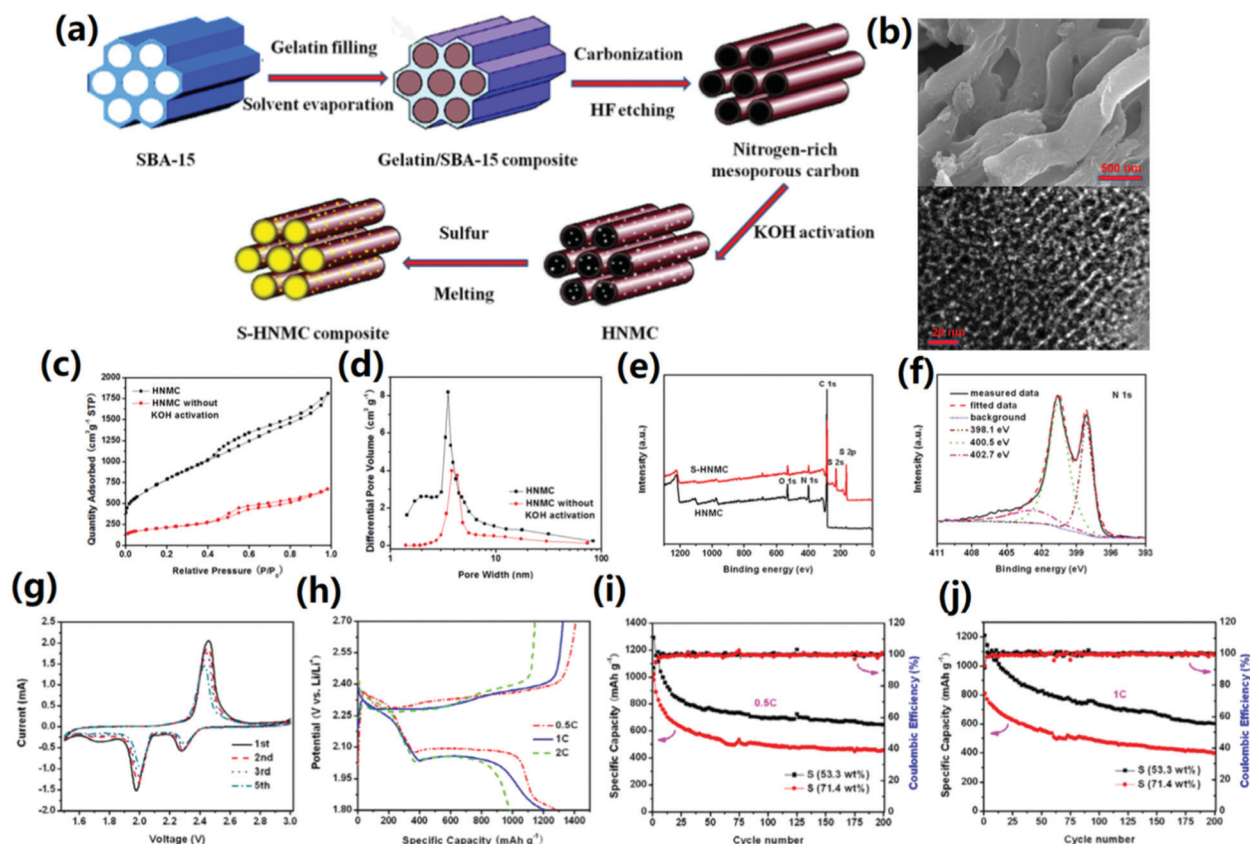


Fig. 13 (a) Schematic illustration of the preparation of the highly ordered nitrogen-rich mesoporous biochar; (b) SEM (up) and TEM (down) images of the as-synthesized biochar material; (c-f) nitrogen adsorption-desorption isotherms, pore size distribution, XPS survey spectra and XPS N 1s spectrum of the biochar materials; and (g-j) performance of the biochar material as a cathode in the LSB: (g) cyclic voltammograms; (h) charge/discharge curves; (i) cycling performance at 0.5C; and (j) cycling performance at 1C (reprinted with permission from ref. 6, copyright 2014 Elsevier Ltd).

the sulfur–biochar composite cathode was attributed to the highly ordered mesoporous structure with abundant nitrogen species biochar. On the one hand, the large specific surface area and abundant ordered mesopore structure could offer proper surfaces and channels to adsorb the *in situ* produced polysulfides, delay the shuttle effect, and improve the infiltration of sulfur into the interior pores. These merits increase the conductivity of insulating sulfur, and provide a stable framework to sustain the strain generated *via* the active material volume changes during the LSB cycling. On the other hand, suitable nitrogen-doping may help biochar to suppress polysulfide species diffusion through enhanced surface adsorption.

However, it should be noted that biochar is not the ultimate solution for Li–S batteries as it could not effectively solve some inherent problems such as a high electrolyte/sulfur ratio and nonstable lithium metal. Meanwhile, biochar materials cannot completely stop polysulfide diffusion out from the cathode composite. More efforts should be made to resolve these problems.

Compared to carbon materials, some metal oxides, such as  $\text{TiO}_2$ ,  $\text{MnO}_2$ , and  $\text{Co}_3\text{O}_4$ , usually have stronger binding energy to the sulfur species, but their electrical conductivity is much worse.<sup>235–237</sup> Therefore, it would be highly desirable to develop hybrid structures combining metal oxides with porous carbon materials for LSB cathodes, which could achieve both strong adsorbability to sulfur or polysulfides and favorable electrical conductivity. Tao *et al.*<sup>8</sup> decorated various nonconductive metal-oxide ( $\text{MgO}$ ,  $\text{Al}_2\text{O}_3$ ,  $\text{CeO}_2$ ,  $\text{La}_2\text{O}_3$  and  $\text{CaO}$ ) nanoparticles onto carbon flakes using Kapok tree fibers as both the template and carbon source (Fig. 14a). The as-synthesized hybrid structures based on  $\text{CeO}_2$ ,  $\text{MgO}$ , and  $\text{La}_2\text{O}_3$  showed a higher capacity and better cycling stability than the other oxides (Fig. 14b and c). Adsorption tests (Fig. 14d) combined with density functional theory (DFT) calculations (Fig. 14e) indicate that better surface diffusion contributes mainly to the higher deposition efficiency of sulfide species.

Although lithium batteries (LIBs and LSBs) have developed very quickly in the past few years, their applications still encounter several challenges such as the scarcity of Li

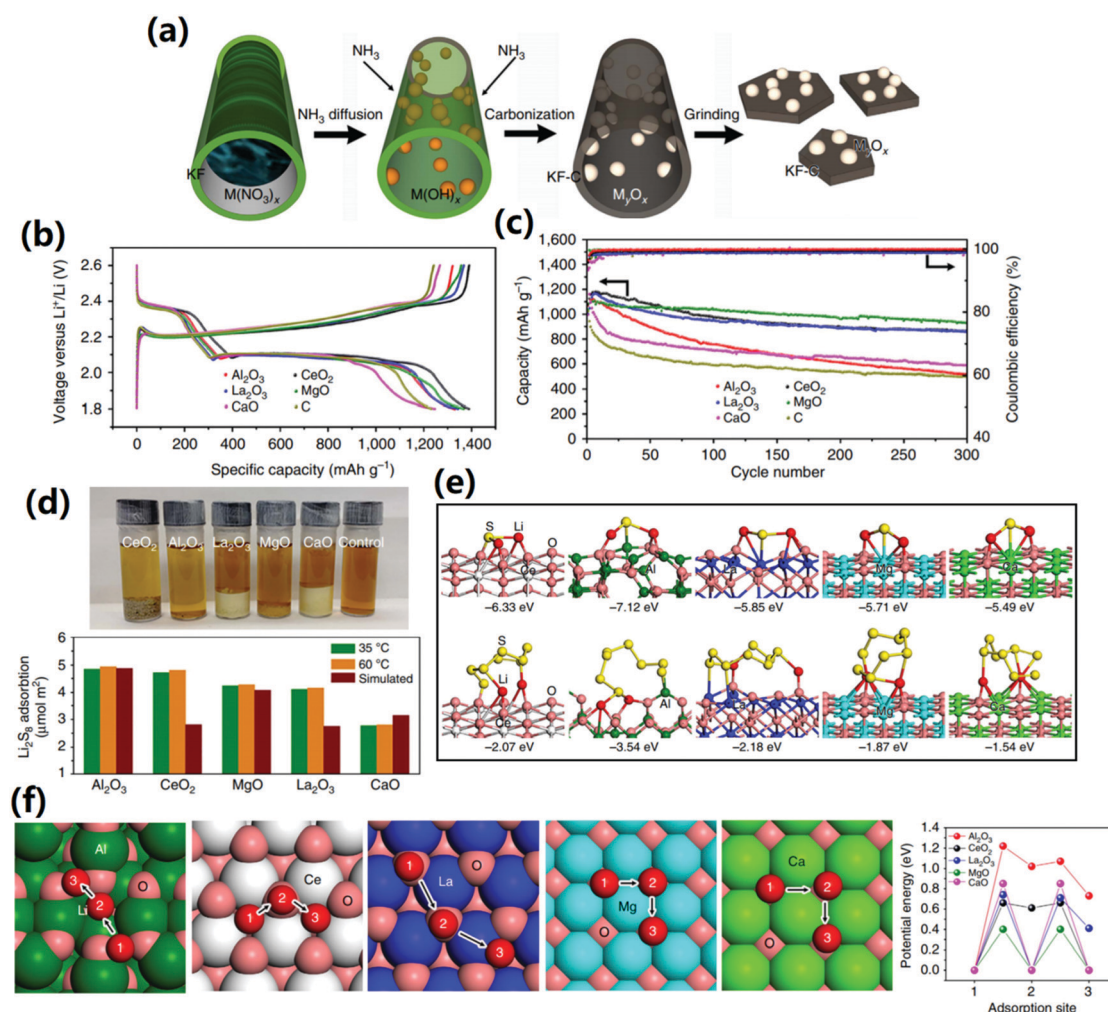


Fig. 14 (a) Schematic illustration of the synthesis of metal oxide/carbon hybrid structures; (b) charge–discharge curves and (c) cycling performance of the hybrid structures electrodes; (d) adsorption test and (e) relative models of sulfide species on the metal oxide surface; and (f) lithium diffusion mechanism and potential energy profiles for  $\text{Li}^+$  diffusion along different adsorption sites on the surface of various metal oxides (reprinted with permission from ref. 8, copyright 2016 from the authors).

resources, engineering difficulties and safety related to Li metal. An appealing alternative to lithium batteries is sodium-ion batteries (SIBs) due to the much greater abundance of Na than the mere 17 ppm of highly unevenly distributed Li in the crust of the Earth.<sup>238</sup> Amorphous porous carbon is a promising anode material for SIBs due to its large interlayer distance and disordered structure.<sup>239</sup> The reasons why amorphous carbon-based electrode materials could enhance the performance of SIBs are their unique physicochemical properties including abundant availability, cost effectiveness, moderate conductivity, relatively high surface area, and excellent corrosion resistance.<sup>240</sup>

As an important source of amorphous porous carbons, biochar-based materials have been widely applied as anode materials of SIBs.<sup>241–247</sup> Li *et al.*<sup>248</sup> synthesized a novel, macroscopic 3D hollow reticulate biochar material by a hydrothermal pretreatment followed by the low temperature (600 °C) pyrolysis method from rape pollen grain biomass. The results show that the hydrothermal pretreatment gets through the reticulate structure by removing flavonoids while the pyrolysis temperature is a key factor for inheriting the unique architecture, as shown in Fig. 15a. When used as an anodic material for SIBs,

the reticulate biochar material (RPC) exhibits excellent cycling stability with a retention capacity of 90% after 1000 cycles (Fig. 15b). This excellent Na-ion storage property can be attributed to the interconnected 3D architecture, the abundant O-containing functional groups and the large interlayer spacing (Fig. 15c). More recent investigations on the applications of biochar based materials in Li and Na batteries have been summarized in Table 6.

## 7. Conclusions and future perspectives

In this review, recent advances in the emerging applications of biochar-based materials for energy storage and conversion, including hydrogen storage and production, ORR and OER catalysts, fuel cells, supercapacitors, and lithium/sodium ion batteries, have been summarized and discussed. Generally, its easily tuned surface chemistry, versatile porous structure, and natural abundance make biochar a promising material for the synthesis of various functional materials that can be applied in emerging energy storage and conversion technologies. In particular, the doping of heteroatoms into the biochar carbon matrix and the synergistic effects between biochar and its loading materials (mainly metals and their oxides) play important roles for improving the performance of biochar-based materials for various energy storage and conversion reactions and processes.

For H<sub>2</sub> energy applications, biochar-based materials exhibit favorable performance in both room temperature and hypothermal H<sub>2</sub> storage owing to its easily tuned porous structure, abundant surface functional groups, and various inorganic species. Physical adsorption *via* the micropore structure and the interaction between H<sub>2</sub> and alkaline or alkaline-earth metal species contribute mainly to hypothermal H<sub>2</sub> storage. Chemical adsorption *via* H<sub>2</sub> spillover effects is mainly responsible for room temperature H<sub>2</sub> storage. Meanwhile, biochar-based materials also play important roles in biological or electrochemical H<sub>2</sub> production as an additive or catalyst. In biological H<sub>2</sub> production, biochar can serve as additives to enhance H<sub>2</sub> production due to its ability to mitigate acid and ammonia inhibition and promote bio-film formation, while in electrochemical H<sub>2</sub> production, doping heteroatoms such as N and S into biochar could remarkably improve the catalytic activity.

In applications as oxygen catalysts, biochar could potentially act as an efficient and sustainable ORR electrocatalyst due to its naturally high levels of heteroatoms such as N, S, and P. Apart from lower production costs, the benefits of biochar-based ORR electrocatalysts include higher stability and better tolerance to CO and methanol compared to the benchmark Pt-based ORR catalysts. Biochar also shows high catalytic activity towards the OER. Doping heteroatoms such as N, S, and P into the biochar matrix and loading metal oxides/carbides into the biochar porous structure are regarded to contribute mainly to the high OER catalytic performance of biochar-based materials.

For fuel cell applications, the poorly crystallized and highly lattice disordered carbons, and high electrical conductivity are

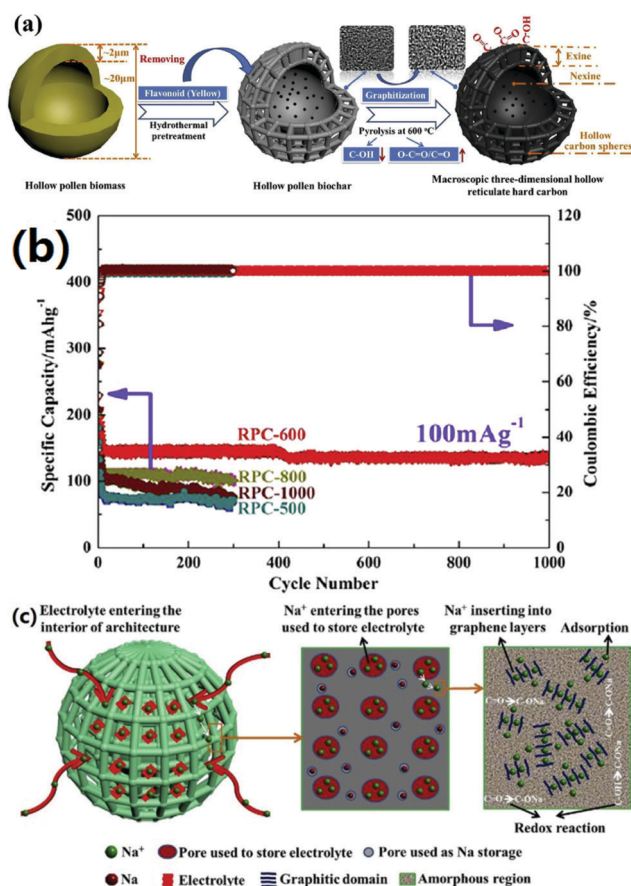


Fig. 15 (a) Schematic illustration of the synthesis of the macroscopic 3D hollow reticulate hard carbon produced from rape pollen grains; (b) cycling performance at 100 mA g<sup>-1</sup> of the materials; and (c) schematic illustration of the discharge process of the RPC-600 anode in SIBs. (Reprinted with permission from ref. 248, Copyright 2017, Elsevier B. V.).

Table 6 Summary of the recent studies on the applications of biochar based materials in Li or Na ion batteries

Original Biomass	Biochar synthesis method	Application	Performance	Ref.
Cattle bone	Pyrolysis of the cattle bone at 600–1200 °C for 2 h	LIBs	Rate capacities: 1230, 951, 682, 491 and 343 mA h g <sup>-1</sup> at 1, 2, 5, 10, 20 A g <sup>-1</sup> ; cycle capacity: 1488 mA h g <sup>-1</sup> after 250 cycles at 1 A g <sup>-1</sup> , and 661 mA h g <sup>-1</sup> after 1500 cycles at 10 A g <sup>-1</sup>	5
Corn stalks	Pyrolysis of the corn stalks with CaCl <sub>2</sub> at 300 °C for 3 h, then activated at 600 °C for 1 h	LIBs	Rate capacities: 1862.1 mA h g <sup>-1</sup> at 0.2C of discharge; 13 cycle capacity: 783.8 mA h g <sup>-1</sup> after 100 cycles	
Kapok fibers	Pyrolysis of the Kapok fibers at 1500 °C for 6 h, then treated with HNO <sub>3</sub> at room temperature for 6 h, and loaded with KMnO <sub>4</sub> /K <sub>2</sub> SO <sub>4</sub> , and heated at 500 °C in H <sub>2</sub> /Ar flow for 5 h to obtain MnO/C	LIBs	Rate capacities: 654, 477, and 65 mA h g <sup>-1</sup> at 0.1, 1, and 20 A g <sup>-1</sup> ; cycle capacity: 371 mA h g <sup>-1</sup> after the 10th cycle at 0.1 A g <sup>-1</sup> , 213 mA h g <sup>-1</sup> after the 40th cycle at 1 A g <sup>-1</sup> , and about 111 mA h g <sup>-1</sup> after the 70th cycle at 10 A g <sup>-1</sup>	20
Apricot shells	Direct pyrolysis of the apricot shell biomass at 900–1500 °C, then treated at 800 °C under Ar/H <sub>2</sub> flow for 2 h	SIBs	Rate capacities: 400 mA h g <sup>-1</sup> with an initial coulombic efficiency of 79%; cycle capacity: 338 mA h g <sup>-1</sup> after 300 cycles	26
Coconut shells	Direct pyrolysis of the coconut shell biomass at 600 °C for 2 h, then activated with KOH at 800 °C for 1 h	LIBs	Rate capacities: 1599 and 1500 mA h g <sup>-1</sup> at current rates of 0.5 and 2.0C; cycle capacity: 517 mA h g <sup>-1</sup> was retained at 2.0C even after 400 cycles	38
Rapeseed pollen	Pyrolysis of the mixture of rapeseed pollen biomass with KMnO <sub>4</sub> at 500 °C under Ar/H <sub>2</sub> flow for 15 h to obtain MnO/C–N nanocomposites	LIBs	Rate capacities: 756.5 mA h g <sup>-1</sup> at 100 mA g <sup>-1</sup> ; cycle capacity: 513.0 mA h g <sup>-1</sup> , ~95.16% of the initial reversible capacity, after 400 cycles at 300 mA g <sup>-1</sup>	45
Dandelions	Pyrolysis of the dandelion biomass at 800–1400 °C for 5 h	SIBs	Rate capacities: 361 mA h g <sup>-1</sup> at 50 mA g <sup>-1</sup> ; cycle capacity: 354.3 mA h g <sup>-1</sup> at 50 mA g <sup>-1</sup> after 10 cycles	58
Yeast cells	Pyrolysis of the mixture of yeast biomass, hexamethylenetetramine, and NiSO <sub>4</sub> at 700 °C for 2 h to obtain Ni(OH) <sub>2</sub> @porous carbon nanocomposites	LSBs	Rate capacities: 1335 mA h g <sup>-1</sup> at 0.1C; cycle capacity: 65 602 mA h g <sup>-1</sup> after 200 cycles at 0.2C	65
Lotus stems	Pyrolysis of the lotus stem biomass at 1200–1600 °C for 5 h	SIBs	Rate capacities: 350 mA h g <sup>-1</sup> at 100 mA g <sup>-1</sup> ; cycle capacity: capacity still retains 94% after 450 cycles at 100 mA g <sup>-1</sup>	71
Apple and celery	Pyrolysis of the apple and celery biomass at 500 °C for 3 h	LIBs	Rate capacities: for apple biochar, 1600, 1470, 1260, 1070 and 1000 mA h g <sup>-1</sup> at 0.074, 0.185, 0.37, 0.74 and 1.11 A g <sup>-1</sup> , for celery biochar, 1620, 1288, 1024, 930 and 850 mA h g <sup>-1</sup> at 0.074, 0.185, 0.37, 0.74 and 1.11 A g <sup>-1</sup> ; cycle capacity: 1050 mA h g <sup>-1</sup> for apple biochar and 990 mA h g <sup>-1</sup> for celery biochar at 100 mA g <sup>-1</sup> after 200 cycles	76
Pinecones	Pyrolysis of the pinecones at 500 °C for 2 h, then activated with KOH for 500–1600 °C for 2 h	SIBs	Rate capacities: 370 mA h g <sup>-1</sup> at 30 mA g <sup>-1</sup> ; cycle capacity: 334 mA h g <sup>-1</sup> after 450 cycles at 100 mA g <sup>-1</sup>	80
Medium-density fiber-board wood	The wood biomass was first impregnated with FeCl <sub>3</sub> solution, then pyrolysis at 500 °C for 30 min, at then at 800–2000 °C for 30 min	LIBs	Rate capacities: 307 mA h g <sup>-1</sup> at 0.1C; cycle capacity: a capacity retention higher than 90% was obtained after 200 cycles	85

mainly responsible for the high performance of biochar-based DCFCs, while the abundant surface functional groups and catalytic effects of some inorganic species like K, Mg, Ca, and Fe in biochar could be a big supplement to DCFCs. In MFC applications, the rational porous structure and high surface area, great conductivity, excellent biocompatibility and abundant availability make biochar-based materials promising MFC anodic materials.

For applications in supercapacitors, biochar-based materials exhibit excellent performance, including large specific capacitance and excellent cycle stability. The capacitive performance of biochar-based materials depends not only on surface area and pore features (pore size and distribution), but also on other factors like electrical conductivity and surface functionalities. Surface doping with heteroatoms such as N, P, and S, and surface combining with metal oxide nanostructures into biochar can introduce pseudocapacitive effects, thus improving the capacitive performance.

In the application of biochar-based materials in Li/Na ion batteries, they act as critical sustainable components for high-performance anodes in LIBs because of their unique surface

chemistry, porous structure, and nanostructure. In particular, heteroatom doping and the synergistic effect between carbons and combined metal/metal oxides play an important role in the improvement of the Li storage capacity and stability.

Although considerable progress has been made in the applications of biochar-based materials for various energy storage and conversion technologies, some critical issues should still be addressed in future work (Fig. 16). First, conventional approaches for biochar functionalization such as surface oxidation, amination, and sulfonation usually involve complex operations or toxic chemicals. Secondly, it is difficult to maintain the conversion efficiency of biomass into biochar without influencing the further treatments of biochar, such as pore and surface chemistry tuning as well as loading of metal and oxides. Thirdly, it is hard to balance the conversion of biomass into biochar-based materials and their applications in energy fields. This is important as it cannot completely remove the impurities in biomass, possibly adversely affecting the performance of the final materials, and also because the expected carbon structure of biochar might not always have positive effects on the performance of the final materials.

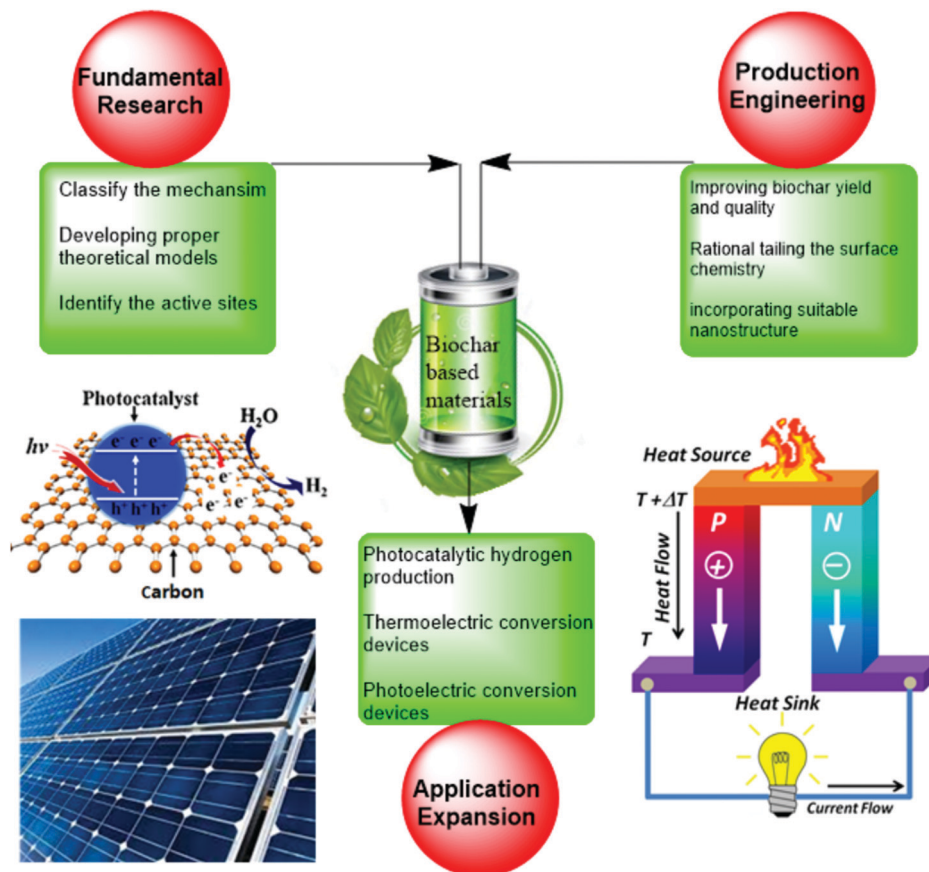


Fig. 16 Outlook and perspective for future work on biochar-based materials in energy storage and conversion applications.

Finally, compared with conventional activated carbon materials, although the surface chemistry and porous structure of biochar could be easily tuned, there is no strong flexibility or ability to composite with other diverse functional materials for further improvement in performance. To address the aforementioned issues, several strategies can be proposed as follows:

(1) For biochar functionalization, more efforts should be directed towards tailoring its fountainhead, the precursor biomass. The components of plant biomass could be tuned to meet the requirements for further biochar functionalization with the help of plant biotechnology. For example, in their growth cycle, apart from water and CO<sub>2</sub>, plants also need to take up many other elements, such as N, P, Mg, S, and microelements, which could be enriched into the plant biomass by tuning the soil properties or adjusting the utilization of fertilizer. As a consequence, when the plant biomass enriched in certain elements is pyrolyzed, resulting biochar with specific functionalities or heteroatom doping could be directly obtained. This can yet be regarded as a more sustainable approach for biochar functionalization than conventional methods.

(2) Developing an easily scaled-up and cost-effective approach to improve the conversion efficiency from biomass to biochar with specific characteristics such as a porous structure, abundant surface functional groups, and a uniform nanostructure. To achieve this goal, properly selecting and

pre-treating before converting the biomass into biochar could be a good option leading to the production of low-cost and high-quality biochar materials with the expected porous structure, surface chemistry and nanostructure.

(3) Developing proper theoretical models concerning the design and synthesis of biochar and its composites with an emphasis on the surface chemistry and molecular interactions, directing researchers to minimize the negative effects related to the impurities on the carbon structure of biochar and its performance in energy conversion and storage.

(4) Selecting suitable components that demonstrate good physicochemical stability and suitable compatibility with carbon to develop high performance biochar-based composites for energy applications. For this purpose, the components should fully utilize the high surface area of biochar while maintaining the structure and porosity of both the components and biochar.

Apart from the aforementioned energy applications, future work should also be devoted to expanding new energy applications of biochar. Photocatalytic H<sub>2</sub> production should be a new direction for the future applications of biochar-based materials. Usually, carbon-based materials are seldom used directly as a photocatalyst for H<sub>2</sub> production from water splitting, but this does not impede the applications of carbon-based materials in photocatalytic H<sub>2</sub> production.<sup>249</sup> Carbon-based materials usually act as a promoter to enhance the performance of semiconductor

photocatalysts. The main roles played by carbon-based materials in photocatalysis include the following five aspects: (1) acting as a catalyst support; (2) increasing the adsorption and active catalytic sites; (3) acting as an electron acceptor or transport channel; (4) increasing the band gap narrowing effects; and (5) acting as a photosensitization agent.<sup>249</sup> Previous studies have indicated that carbon nanotubes,<sup>250</sup> graphene,<sup>251</sup> and carbon quantum dots<sup>252</sup> can be used as co-catalysts or a promoter in photocatalytic H<sub>2</sub> production. A great advancement would be to replace the aforementioned expensive carbon materials with sustainable and cost-effective biochar-based materials, which could bring many environmental and economic benefits. Future work should be devoted to this topic. Energy storage and conversion devices should be another new direction. Conventional carbon materials are important components in many energy storage and conversion devices such as photoelectric conversion<sup>253–257</sup> and thermo-electric conversion devices.<sup>258–261</sup> Using biochar-based materials as an alternative to conventional carbon materials in the aforementioned devices should be a future research direction for expanding the energy applications of biochar-based materials.

Although there will be great challenges in expanding the use of biochar in energy applications, the current accomplishments achieved are very inspiring and comprehensive. With continual research contributions on this research topic, there could be great opportunities to achieve practical applications of biochar materials in the fields of renewable energy conversion and storage. We hope that this review not only provides the reader with a good overview of the current advances in the energy applications of biochar-based materials but also highlights some goals and challenges remaining in the future research development of this topic.

## Conflicts of interest

There are no conflicts to declare.

## Acknowledgements

The authors gratefully acknowledge the financial support from the National Natural Science Foundation of China (21607147, 51538011 and 51821006), Program for Changjiang Scholars and Innovative Research Team at the University of the Ministry of Education of China, China.

## Notes and references

- M. Fowles, *Biomass Bioenergy*, 2007, **31**, 426–432.
- F. Pan, Z. Cao, Q. Zhao, H. Liang and J. Zhang, *J. Power Sources*, 2014, **272**, 8–15.
- L. Chen, Y. Zhang, C. Lin, W. Yang, Y. Meng, Y. Guo, M. Li and D. Xiao, *J. Mater. Chem. A*, 2014, **2**, 9684–9690.
- H. Akasaka, T. Takahata, I. Toda, H. Ono, S. Ohshio, S. Himeno, T. Kokubu and H. Saitoh, *Int. J. Hydrogen Energy*, 2011, **36**, 580–585.
- J. Niu, R. Shao, J. Liang, M. Dou, Z. Li, Y. Huang and F. Wang, *Nano Energy*, 2017, **36**, 322–330.
- Y. Qu, Z. Zhang, X. Zhang, G. Ren, Y. Lai, Y. Liu and J. Li, *Carbon*, 2015, **84**, 399–408.
- W. Cai, J. Liu, P. Liu, Z. Liu, H. Xu, B. Chen, Y. Li, Q. Zhou, M. Liu and M. Ni, *Int. J. Energy Res.*, 2018, **42**, 1–10.
- X. Tao, J. Wang, C. Liu, H. Wang, H. Yao, G. Zheng, Z. W. Seh, Q. Cai, W. Li and G. Zhou, *Nat. Commun.*, 2016, **7**, 11203.
- X. Fan, C. Yu, J. Yang, Z. Ling, C. Hu, M. Zhang and J. Qiu, *Adv. Energy Mater.*, 2015, **5**, 1401761.
- Y. Zhou, Y. Leng, W. Zhou, J. Huang, M. Zhao, J. Zhan, C. Feng, Z. Tang, S. Chen and H. Liu, *Nano Energy*, 2015, **16**, 357–366.
- V. V. Bhat, C. I. Contescu, N. C. Gallego and F. S. Baker, *Carbon*, 2010, **48**, 1331–1340.
- C. Guo, W. Liao, Z. Li and C. Chen, *Carbon*, 2015, **85**, 279–288.
- Y. Li, C. Li, H. Qi, K. Yu and X. Li, *RSC Adv.*, 2018, **8**, 12666–12671.
- J. Li, B. Wei, C. Wang, Z. Zhou and Z. Lü, *Int. J. Hydrogen Energy*, 2018, **43**, 12358–12367.
- Y. S. Yun, S. Y. Cho, J. Shim, B. H. Kim, S. J. Chang, S. J. Baek, Y. S. Huh, Y. Tak, Y. W. Park and S. Park, *Adv. Mater.*, 2013, **25**, 1993–1998.
- Y. Sun and P. A. Webley, *Chem. Eng. J.*, 2010, **162**, 883–892.
- M. P. Suh, H. J. Park, T. K. Prasad and D.-W. Lim, *Chem. Rev.*, 2012, **112**, 782–835.
- M. Li, Y. Xiong, X. Liu, C. Han, Y. Zhang, X. Bo and L. Guo, *J. Mater. Chem. A*, 2015, **3**, 9658–9667.
- W. An, X. Sun, Y. Jiao, S. Wang, W. Wang, M. O. Tade, Z. Shao, S.-D. Li and S. Shuang, *Energy Fuels*, 2018, **32**, 4559–4568.
- Y. Zhao, Y. Cui, J. Shi, W. Liu, Z. Shi, S. Chen, X. Wang and H. Wang, *J. Mater. Chem. A*, 2017, **5**, 15243–15252.
- C. Chen, D. Yu, G. Zhao, B. Du, W. Tang, L. Sun, Y. Sun, F. Besenbacher and M. Yu, *Nano Energy*, 2016, **27**, 377–389.
- R. Yang, G. Liu, M. Li, J. Zhang and X. Hao, *Microporous Mesoporous Mater.*, 2012, **158**, 108–116.
- K. Wang, H. Wang, S. Ji, H. Feng, V. Linkov and R. Wang, *RSC Adv.*, 2013, **3**, 12039–12042.
- M. Konsolakis, N. Kakkidid, G. E. Marnellos, D. Zaharaki and K. Komnitsas, *RSC Adv.*, 2015, **5**, 73399–73409.
- Q. Zhang, E. Uchaker, S. L. Candelaria and G. Cao, *Chem. Soc. Rev.*, 2013, **42**, 3127–3171.
- Y. Zhu, M. Chen, Q. Li, C. Yuan and C. Wang, *Carbon*, 2018, **129**, 695–701.
- W. Tian, Q. Gao, Y. Tan, K. Yang, L. Zhu, C. Yang and H. Zhang, *J. Mater. Chem. A*, 2015, **3**, 5656–5664.
- A. Ariharan and B. Viswanathan, *Int. J. Hydrogen Energy*, 2018, **43**, 5077–5088.
- X. Liu, Y. Zhou, W. Zhou, L. Li, S. Huang and S. Chen, *Nanoscale*, 2015, **7**, 6136–6142.
- Q. Zhou, W. Cai, Y. Zhang, J. Liu, L. Yuan, F. Yu, X. Wang and M. Liu, *Biomass Bioenergy*, 2016, **91**, 250–258.
- H. Nishihara and T. Kyotani, *Adv. Mater.*, 2012, **24**, 4473–4498.

- 32 Y. Li and Z. Chen, *Graphene Chemistry*, John Wiley & Sons, Ltd, 2013, pp. 371–391, DOI: 10.1002/9781118691281.ch16.
- 33 A. Linares-Solano, M. Jordá-Beneyto, D. Lozano-Castelló, F. Suárez-García and D. Cazorla-Amorós, *Materials Innovations in an Emerging Hydrogen Economy*, John Wiley & Sons, Inc., 2008, pp. 77–90, DOI: 10.1002/9780470483428.ch8.
- 34 L. Zhang, J. Xiao, H. Wang and M. Shao, *ACS Catal.*, 2017, 7, 7855–7865.
- 35 L. Dai, Y. Xue, L. Qu, H.-J. Choi and J.-B. Baek, *Chem. Rev.*, 2015, 115, 4823–4892.
- 36 D. S. Su, S. Perathoner and G. Centi, *Chem. Rev.*, 2013, 113, 5782–5816.
- 37 T. S. Blankenship II, N. Balahmar and R. Mokaya, *Nat. Commun.*, 2017, 8, 1545.
- 38 Z.-H. Chen, X.-L. Du, J.-B. He, F. Li, Y. Wang, Y.-L. Li, B. Li and S. Xin, *ACS Appl. Mater. Interfaces*, 2017, 9, 33855–33862.
- 39 A. D. Roberts, X. Li and H. Zhang, *Chem. Soc. Rev.*, 2014, 43, 4341–4356.
- 40 L. L. Zhang and X. S. Zhao, *Chem. Soc. Rev.*, 2009, 38, 2520–2531.
- 41 M. Yang, D. S. Kim, S. B. Hong, J.-W. Sim, J. Kim, S.-S. Kim and B. G. Choi, *Langmuir*, 2017, 33, 5140–5147.
- 42 C. Guo, W. Liao, Z. Li, L. Sun and C. Chen, *Nanoscale*, 2015, 7, 15990–15998.
- 43 J. Zhang, Z. Zhong, D. Shen, J. Zhao, H. Zhang, M. Yang and W. Li, *Energy Fuels*, 2011, 25, 2187–2193.
- 44 J. Zhang, C. Fan, H. Zhang, Z. Wang, J. Zhang and M. Song, *Int. J. Hydrogen Energy*, 2018, 43, 8729–8738.
- 45 L.-F. Chen, S.-X. Ma, S. Lu, Y. Feng, J. Zhang, S. Xin and S.-H. Yu, *Nano Res.*, 2017, 10, 1–11.
- 46 X.-L. Wu, T. Wen, H.-L. Guo, S. Yang, X. Wang and A.-W. Xu, *ACS Nano*, 2013, 7, 3589–3597.
- 47 Y. Ma, J. Zhao, L. Zhang, Y. Zhao, Q. Fan, X. A. Li, Z. Hu and W. Huang, *Carbon*, 2011, 49, 5292–5297.
- 48 G. Yue, K. Meng and Q. Liu, *ChemPlusChem*, 2015, 80, 1133–1138.
- 49 M.-M. Titirici, R. J. White, N. Brun, V. L. Budarin, D. S. Su, F. del Monte, J. H. Clark and M. J. MacLachlan, *Chem. Soc. Rev.*, 2015, 44, 250–290.
- 50 R. Garg, S. Elmas, T. Nann and M. R. Andersson, *Adv. Energy Mater.*, 2017, 7, 1601393.
- 51 Y.-L. Li, I. A. Kinloch and A. H. Windle, *Science*, 2004, 304, 276–278.
- 52 Y. Saito, T. Nakahira and S. Uemura, *J. Phys. Chem. B*, 2003, 107, 931–934.
- 53 P. Chingombe, B. Saha and R. Wakeman, *Carbon*, 2005, 43, 3132–3143.
- 54 G. Zhu, L. Ma, H. Lv, Y. Hu, T. Chen, R. Chen, J. Liang, X. Wang, Y. Wang and C. Yan, *Nanoscale*, 2017, 9, 1237–1243.
- 55 J. Liu, Y. Deng, X. Li and L. Wang, *ACS Sustainable Chem. Eng.*, 2016, 4, 177–187.
- 56 T. Huggins, A. Latorre, J. Biffinger and Z. Ren, *Sustainability*, 2016, 8, 169.
- 57 W. Wan, Q. Wang, L. Zhang, H.-W. Liang, P. Chen and S.-H. Yu, *J. Mater. Chem. A*, 2016, 4, 8602–8609.
- 58 C. Wang, J. Huang, H. Qi, L. Cao, Z. Xu, Y. Cheng, X. Zhao and J. Li, *J. Power Sources*, 2017, 358, 85–92.
- 59 F. Liu, H. Peng, X. Qiao, Z. Fu, P. Huang and S. Liao, *Int. J. Hydrogen Energy*, 2014, 39, 10128–10134.
- 60 G. Zhou, Q. Yang, X. Guo, Y. Chen, Q. Yang, L. Xu, D. Sun and Y. Tang, *Int. J. Hydrogen Energy*, 2018, 43, 9326–9333.
- 61 L. Deng, Y. Yuan, Y. Zhang, Y. Wang, Y. Chen, H. Yuan and Y. Chen, *ACS Sustainable Chem. Eng.*, 2017, 5, 9766–9773.
- 62 N. Guo, M. Li, Y. Wang, X. Sun, F. Wang and R. Yang, *ACS Appl. Mater. Interfaces*, 2016, 8, 33626–33634.
- 63 T. Wakamatsu and Y. Numata, *Miner. Eng.*, 1991, 4, 975–982.
- 64 D. Zhao, Y. Zhang and E. J. Essene, *Ore Geol. Rev.*, 2015, 65, 733–748.
- 65 Y. Xia, H. Zhong, R. Fang, C. Liang, Z. Xiao, H. Huang, Y. Gan, J. Zhang, X. Tao and W. Zhang, *J. Power Sources*, 2018, 378, 73–80.
- 66 M. Wang, Y. Lai, J. Fang, J. Li, F. Qin, K. Zhang and H. Lu, *Int. J. Hydrogen Energy*, 2015, 40, 16230–16237.
- 67 M. Karnan, K. Subramani, N. Sudhan, N. Ilayaraja and M. Sathish, *ACS Appl. Mater. Interfaces*, 2016, 8, 35191–35202.
- 68 B. Wang, L. Xu, G. Liu, P. Zhang, W. Zhu, J. Xia and H. Li, *J. Mater. Chem. A*, 2017, 5, 20170–20179.
- 69 J. Md Khudzari, Y. Gariépy, J. Kurian, B. Tartakovsky and G. S. V. Raghavan, *Biochem. Eng. J.*, 2019, 141, 190–199.
- 70 Y. M. Bar-On, R. Phillips and R. Milo, *Proc. Natl. Acad. Sci. U. S. A.*, 2018, 201711842.
- 71 N. Zhang, Q. Liu, W. Chen, M. Wan, X. Li, L. Wang, L. Xue and W. Zhang, *J. Power Sources*, 2018, 378, 331–337.
- 72 M. Borghei, N. Laocharoen, E. Kibena-Pöldsepp, L.-S. Johansson, J. Campbell, E. Kauppinen, K. Tammeveski and O. J. Rojas, *Appl. Catal., B*, 2017, 204, 394–402.
- 73 C. Wu, S. Yang, J. Cai, Q. Zhang, Y. Zhu and K. Zhang, *ACS Appl. Mater. Interfaces*, 2016, 8, 15288–15296.
- 74 M. Li, H. Zhang, T. Xiao, S. Wang, B. Zhang, D. Chen, M. Su and J. Tang, *Electrochim. Acta*, 2018, 283, 780–788.
- 75 H. Zhou, J. Zhang, J. Zhu, Z. Liu, C. Zhang and S. Mu, *RSC Adv.*, 2016, 6, 73292–73300.
- 76 J. Hao, Y. Wang, C. Chi, J. Wang, Q. Guo, Y. Yang, Y. Li, X. Liu and J. Zhao, *Sustainable Energy Fuels*, 2018, 2, 2358–2365.
- 77 W.-J. Liu, H. Jiang and H.-Q. Yu, *Chem. Rev.*, 2015, 115, 12251–12285.
- 78 H. Wang, Z. Xu, A. Kohandehghan, Z. Li, K. Cui, X. Tan, T. J. Stephenson, C. K. King'ondeu, C. M. B. Holt, B. C. Olsen, J. K. Tak, D. Harfield, A. O. Anyia and D. Mitlin, *ACS Nano*, 2013, 7, 5131–5141.
- 79 C. Sophia Ayyappan, V. M. Bhalambal and S. Kumar, *Bioresour. Technol.*, 2018, 251, 165–170.
- 80 T. Zhang, J. Mao, X. Liu, M. Xuan, K. Bi, X. L. Zhang, J. Hu, J. Fan, S. Chen and G. Shao, *RSC Adv.*, 2017, 7, 41504–41511.
- 81 M. Zhang, X. Jin, L. Wang, M. Sun, Y. Tang, Y. Chen, Y. Sun, X. Yang and P. Wan, *Appl. Surf. Sci.*, 2017, 411, 251–260.

- 82 D. Woolf, J. E. Amonette, F. A. Street-Perrott, J. Lehmann and S. Joseph, *Nat. Commun.*, 2010, **1**, 56.
- 83 W.-J. Liu, K. Tian, Y.-R. He, H. Jiang and H.-Q. Yu, *Environ. Sci. Technol.*, 2014, **48**, 13951–13959.
- 84 B. Liang, K. Li, Y. Liu and X. Kang, *Chem. Eng. J.*, 2019, **358**, 1002–1011.
- 85 A. Gomez-Martin, J. Martinez-Fernandez, M. Rutttert, A. Heckmann, M. Winter, T. Placke and J. Ramirez-Rico, *ChemSusChem*, 2018, **11**, 2776–2787.
- 86 F. Liu, H. Peng, C. You, Z. Fu, P. Huang, H. Song and S. Liao, *Electrochim. Acta*, 2014, **138**, 353–359.
- 87 W.-J. Liu, K. Tian, L. L. Ling, H.-Q. Yu and H. Jiang, *Environ. Sci. Technol.*, 2016, **50**, 12421–12428.
- 88 L. Zhao, *RSC Adv.*, 2017, **7**, 13904–13910.
- 89 F. M. Gírio, C. Fonseca, F. Carvalheiro, L. C. Duarte, S. Marques and R. Bogel-Lukasik, *Bioresour. Technol.*, 2010, **101**, 4775–4800.
- 90 P. L. Dhepe and A. Fukuoka, *ChemSusChem*, 2008, **1**, 969–975.
- 91 R. Rinaldi and F. Schüth, *ChemSusChem*, 2009, **2**, 1096–1107.
- 92 J. Zakzeski, P. C. A. Bruijninx, A. L. Jongerius and B. M. Weckhuysen, *Chem. Rev.*, 2010, **110**, 3552–3599.
- 93 Y. Gong, D. Li, C. Luo, Q. Fu and C. Pan, *Green Chem.*, 2017, **19**, 4132–4140.
- 94 E. Raymundo-Piñero, M. Cadek and F. Béguin, *Adv. Funct. Mater.*, 2009, **19**, 1032–1039.
- 95 D. A. Laird, R. C. Brown, J. E. Amonette and J. Lehmann, *Biofuels, Bioprod. Biorefin.*, 2009, **3**, 547–562.
- 96 T. R. Brown, M. M. Wright and R. C. Brown, *Biofuels, Bioprod. Biorefin.*, 2011, **5**, 54–68.
- 97 M. Biswal, A. Banerjee, M. Deo and S. Ogale, *Energy Environ. Sci.*, 2013, **6**, 1249–1259.
- 98 G. Wang, L. Zhang and J. Zhang, *Chem. Soc. Rev.*, 2012, **41**, 797–828.
- 99 J. J. Manyà, *Environ. Sci. Technol.*, 2012, **46**, 7939–7954.
- 100 S. Meyer, B. Glaser and P. Quicker, *Environ. Sci. Technol.*, 2011, **45**, 9473–9483.
- 101 C. Hyland and A. K. Sarmah, in *Bioenergy Research: Advances and Applications*, ed. V. K. Gupta, M. G. T. P. Kubicek and J. S. Xu, Elsevier, Amsterdam, 2014, pp. 435–446, DOI: 10.1016/B978-0-444-59561-4.00025-5.
- 102 J. Lee, K.-H. Kim and E. E. Kwon, *Renewable Sustainable Energy Rev.*, 2017, **77**, 70–79.
- 103 X. Xiong, I. K. M. Yu, L. Cao, D. C. W. Tsang, S. Zhang and Y. S. Ok, *Bioresour. Technol.*, 2017, **246**, 254–270.
- 104 A. M. Abioye and F. N. Ani, *Renewable Sustainable Energy Rev.*, 2015, **52**, 1282–1293.
- 105 W. Long, B. Fang, A. Ignaszak, Z. Wu, Y.-J. Wang and D. Wilkinson, *Chem. Soc. Rev.*, 2017, **46**, 7176–7190.
- 106 Y. Yao and F. Wu, *Nano Energy*, 2015, **17**, 91–103.
- 107 Y. Bai, Y. Dou, L.-H. Xie, W. Rutledge, J.-R. Li and H.-C. Zhou, *Chem. Soc. Rev.*, 2016, **45**, 2327–2367.
- 108 H. Zhang, J. Nai, L. Yu and X. W. Lou, *Joule*, 2017, **1**, 77–107.
- 109 G. J. Kubas, *Chem. Rev.*, 2007, **107**, 4152–4205.
- 110 G. Sethia and A. Sayari, *Carbon*, 2016, **99**, 289–294.
- 111 R. Roszak, L. Firlej, S. Roszak, P. Pfeifer and B. Kuchta, *Colloids Surf., A*, 2016, **496**, 69–76.
- 112 Y. Xia, Z. Yang and Y. Zhu, *J. Mater. Chem. A*, 2013, **1**, 9365–9381.
- 113 H. Marsh and F. R. Reinoso, *Activated carbon*, Elsevier, 2006.
- 114 D. F. Quinn and J. A. MacDonald, *Carbon*, 1992, **30**, 1097–1103.
- 115 A. Dillon and M. Heben, *Appl. Phys. A: Mater. Sci. Process.*, 2001, **72**, 133–142.
- 116 A. Züttel, P. Sudan, P. Mauron, T. Kiyobayashi, C. Emmenegger and L. Schlapbach, *Int. J. Hydrogen Energy*, 2002, **27**, 203–212.
- 117 R. Ströbel, J. Garche, P. Moseley, L. Jörissen and G. Wolf, *J. Power Sources*, 2006, **159**, 781–801.
- 118 Y. Xiao, H. Dong, C. Long, M. Zheng, B. Lei, H. Zhang and Y. Liu, *Int. J. Hydrogen Energy*, 2014, **39**, 11661–11667.
- 119 F. Zhang, H. Ma, J. Chen, G.-D. Li, Y. Zhang and J.-S. Chen, *Bioresour. Technol.*, 2008, **99**, 4803–4808.
- 120 F. Cheng, J. Liang, J. Zhao, Z. Tao and J. Chen, *Chem. Mater.*, 2008, **20**, 1889–1895.
- 121 M. Sevilla and R. Mokaya, *Energy Environ. Sci.*, 2014, **7**, 1250–1280.
- 122 H. Jin, Y. S. Lee and I. Hong, *Catal. Today*, 2007, **120**, 399–406.
- 123 L. Wang and R. T. Yang, *Energy Environ. Sci.*, 2008, **1**, 268–279.
- 124 H. Cheng, L. Chen, A. C. Cooper, X. Sha and G. P. Pez, *Energy Environ. Sci.*, 2008, **1**, 338–354.
- 125 L. Wang and R. T. Yang, *Energy Environ. Sci.*, 2008, **1**, 268–279.
- 126 L. Wang and R. T. Yang, *Energy Environ. Sci.*, 2008, **1**, 268–279.
- 127 C.-K. Back, G. Sandí, J. Prakash and J. Hranisavljevic, *J. Phys. Chem. B*, 2006, **110**, 16225–16231.
- 128 V. V. Bhat, C. I. Contescu and N. C. Gallego, *Carbon*, 2010, **48**, 2361–2364.
- 129 Y. E. Cheon and M. P. Suh, *Angew. Chem., Int. Ed.*, 2009, **48**, 2899–2903.
- 130 J. Costerton, *The biofilm primer*, Springer Series on biofilms, Springer, Berlin Heidelberg, New York, 2007, vol. 1.
- 131 Z. Lewandowski and J. P. Boltz, *Treatise on Water Science*, Elsevier, Oxford, 2011, pp. 529–570, DOI: 10.1016/B978-0-444-53199-5.00095-6.
- 132 P. Sharma and U. Melkania, *Int. J. Hydrogen Energy*, 2017, **42**, 18865–18874.
- 133 J. Zhang, C. Fan and L. Zang, *Bioresour. Technol.*, 2017, **245**, 98–105.
- 134 N. M. S. Sunyoto, M. Zhu, Z. Zhang and D. Zhang, *J. Energy Resour. Technol.*, 2018, **140**, 062204.
- 135 J. Zhang, W. Zhao, H. Zhang, Z. Wang, C. Fan and L. Zang, *Bioresour. Technol.*, 2018, **266**, 555–567.
- 136 G. Wang, Q. Li, X. Gao and X. C. Wang, *Bioresour. Technol.*, 2018, **250**, 812–820.
- 137 J.-H. Park, H.-J. Kang, K.-H. Park and H.-D. Park, *Bioresour. Technol.*, 2018, **254**, 300–311.

- 138 G. Yang and J. Wang, *Renewable Sustainable Energy Rev.*, 2018, **95**, 130–146.
- 139 Y. Lin, Y. Pan and J. Zhang, *Electrochim. Acta*, 2017, **232**, 561–569.
- 140 X. Liu, M. Zhang, D. Yu, T. Li, M. Wan, H. Zhu, M. Du and J. Yao, *Electrochim. Acta*, 2016, **215**, 223–230.
- 141 W. Cui, Q. Liu, Z. Xing, A. M. Asiri, K. A. Alamry and X. Sun, *Appl. Catal., B*, 2015, **164**, 144–150.
- 142 F. Lai, Y.-E. Miao, Y. Huang, Y. Zhang and T. Liu, *ACS Appl. Mater. Interfaces*, 2016, **8**, 3558–3566.
- 143 W.-F. Chen, S. Iyer, S. Iyer, K. Sasaki, C.-H. Wang, Y. Zhu, J. T. Muckerman and E. Fujita, *Energy Environ. Sci.*, 2013, **6**, 1818–1826.
- 144 K. An, X. Xu and X.-X. Liu, *ACS Sustainable Chem. Eng.*, 2017, **6**, 1446–1455.
- 145 Y. Zhang, L. Zuo, L. Zhang, Y. Huang, H. Lu, W. Fan and T. Liu, *ACS Appl. Mater. Interfaces*, 2016, **8**, 7077–7085.
- 146 B. Seo, Y. J. Sa, J. Woo, K. Kwon, J. Park, T. J. Shin, H. Y. Jeong and S. H. Joo, *ACS Catal.*, 2016, **6**, 4347–4355.
- 147 Y. G. Zhu, X. Wang, C. Jia, J. Yang and Q. Wang, *ACS Catal.*, 2016, **6**, 6191–6197.
- 148 W. T. Hong, M. Risch, K. A. Stoerzinger, A. Grimaud, J. Suntivich and Y. Shao-Horn, *Energy Environ. Sci.*, 2015, **8**, 1404–1427.
- 149 M. Shao, Q. Chang, J.-P. Dodelet and R. Chenitz, *Chem. Rev.*, 2016, **116**, 3594–3657.
- 150 Y.-J. Wang, N. Zhao, B. Fang, H. Li, X. T. Bi and H. Wang, *Chem. Rev.*, 2015, **115**, 3433–3467.
- 151 K. Gong, F. Du, Z. Xia, M. Durstock and L. Dai, *Science*, 2009, **323**, 760–764.
- 152 M. Borghesi, J. Lehtonen, L. Liu and O. J. Rojas, *Adv. Mater.*, 2017, 1703691.
- 153 P. Chen, L.-K. Wang, G. Wang, M.-R. Gao, J. Ge, W.-J. Yuan, Y.-H. Shen, A.-J. Xie and S.-H. Yu, *Energy Environ. Sci.*, 2014, **7**, 4095–4103.
- 154 Q. Liu, C. Chen, F. Pan and J. Zhang, *Electrochim. Acta*, 2015, **170**, 234–241.
- 155 M. Graglia, J. Pampel, T. Hantke, T.-P. Feller and D. Esposito, *ACS Nano*, 2016, **10**, 4364–4371.
- 156 S. Gao, H. Liu, K. Geng and X. Wei, *Nano Energy*, 2015, **12**, 785–793.
- 157 W. Yang, X. Liu, X. Yue, J. Jia and S. Guo, *J. Am. Chem. Soc.*, 2015, **137**, 1436–1439.
- 158 R. Imran Jafri, N. Rajalakshmi and S. Ramaprabhu, *J. Mater. Chem.*, 2010, **20**, 7114–7117.
- 159 F. Su, Z. Tian, C. K. Poh, Z. Wang, S. H. Lim, Z. Liu and J. Lin, *Chem. Mater.*, 2010, **22**, 832–839.
- 160 L. Xiong, J.-J. Chen, Y.-X. Huang, W.-W. Li, J.-F. Xie and H.-Q. Yu, *Nano Energy*, 2015, **12**, 33–42.
- 161 T. Zhou, H. Wang, S. Ji, V. Linkov and R. Wang, *J. Power Sources*, 2014, **248**, 427–433.
- 162 Y.-J. Wang, D. P. Wilkinson and J. Zhang, *Chem. Rev.*, 2011, **111**, 7625–7651.
- 163 H. Wang, F.-X. Yin, B.-H. Chen, X.-B. He, P.-L. Lv, C.-Y. Ye and D.-J. Liu, *Appl. Catal., B*, 2017, **205**, 55–67.
- 164 G. Wang, Y. Deng, J. Yu, L. Zheng, L. Du, H. Song and S. Liao, *ACS Appl. Mater. Interfaces*, 2017, **9**, 32168–32178.
- 165 I. S. Amini, J. Zhang, Z. Kou, X. Liu, O. K. Asare, H. Zhou, K. Cheng, H. Zhang, L. Mai, M. Pan and S. Mu, *ACS Appl. Mater. Interfaces*, 2016, **8**, 29408–29418.
- 166 A. Elleuch, A. Boussetta, J. Yu, K. Halouani and Y. Li, *Int. J. Hydrogen Energy*, 2013, **38**, 16590–16604.
- 167 J. Yu, Y. Zhao and Y. Li, *J. Power Sources*, 2014, **270**, 312–317.
- 168 N. J. Cherepy, R. Krueger, K. J. Fiet, A. F. Jankowski and J. F. Cooper, *J. Electrochem. Soc.*, 2005, **152**, A80–A87.
- 169 A. Kacprzak, R. Kobylecki, R. Włodarczyk and Z. Bis, *J. Power Sources*, 2014, **255**, 179–186.
- 170 T. M. Gür, *Chem. Rev.*, 2013, **113**, 6179–6206.
- 171 A. C. Rady, S. Giddey, S. P. Badwal, B. P. Ladewig and S. Bhattacharya, *Energy Fuels*, 2012, **26**, 1471–1488.
- 172 N. Jafri, W. Wong, V. Doshi, L. Yoon and K. Cheah, *Process Saf. Environ. Prot.*, 2018, **118**, 152–166.
- 173 D. Cao, Y. Sun and G. Wang, *J. Power Sources*, 2007, **167**, 250–257.
- 174 X. Li, Z. H. Zhu, R. D. Marco, A. Dicks, J. Bradley, S. Liu and G. Q. Lu, *Ind. Eng. Chem. Res.*, 2008, **47**, 9670–9677.
- 175 M. Chen, C. Wang, X. Niu, S. Zhao, J. Tang and B. Zhu, *Int. J. Hydrogen Energy*, 2010, **35**, 2732–2736.
- 176 X. Li, Z. Zhu, J. Chen, R. De Marco, A. Dicks, J. Bradley and G. Lu, *J. Power Sources*, 2009, **186**, 1–9.
- 177 X. Li, Z. Zhu, R. D. Marco, J. Bradley and A. Dicks, *Energy Fuels*, 2009, **23**, 3721–3731.
- 178 C. A. Mullen, A. A. Boateng, N. M. Goldberg, I. M. Lima, D. A. Laird and K. B. Hicks, *Biomass Bioenergy*, 2010, **34**, 67–74.
- 179 X. Li, Z. Zhu, R. De Marco, J. Bradley and A. Dicks, *J. Power Sources*, 2010, **195**, 4051–4058.
- 180 C. Li, Y. Shi and N. Cai, *J. Power Sources*, 2010, **195**, 4660–4666.
- 181 S. Y. Ahn, S. Y. Eom, Y. H. Rhie, Y. M. Sung, C. E. Moon, G. M. Choi and D. J. Kim, *Appl. Energy*, 2013, **105**, 207–216.
- 182 A. Elleuch, A. Boussetta, K. Halouani and Y. Li, *Int. J. Hydrogen Energy*, 2013, **38**, 16605–16614.
- 183 H. Liu, R. Ramnarayanan and B. E. Logan, *Environ. Sci. Technol.*, 2004, **38**, 2281–2285.
- 184 X.-W. Liu, W.-W. Li and H.-Q. Yu, *Chem. Soc. Rev.*, 2014, **43**, 7718–7745.
- 185 H. Wang, J.-D. Park and Z. J. Ren, *Environ. Sci. Technol.*, 2015, **49**, 3267–3277.
- 186 T. Huggins, H. Wang, J. Kearns, P. Jenkins and Z. J. Ren, *Bioresour. Technol.*, 2014, **157**, 114–119.
- 187 Q. Liu, Y. Zhou, S. Chen, Z. Wang, H. Hou and F. Zhao, *J. Power Sources*, 2015, **273**, 1189–1193.
- 188 Y. Yuan, T. Yuan, D. Wang, J. Tang and S. Zhou, *Bioresour. Technol.*, 2013, **144**, 115–120.
- 189 A. Janicek, N. Gao, Y. Fan and H. Liu, *Fuel Cells*, 2015, **15**, 855–861.
- 190 X. Zhang, D. Pant, F. Zhang, J. Liu, W. He and B. E. Logan, *ChemElectroChem*, 2014, **1**, 1859–1866.

- 191 X. Zhang, X. Xia, I. Ivanov, X. Huang and B. E. Logan, *Environ. Sci. Technol.*, 2014, **48**, 2075–2081.
- 192 J. R. Miller and P. Simon, *Science*, 2008, **321**, 651–652.
- 193 R. Mysyk, E. Raymundo-Piñero, M. Anouti, D. Lemordant and F. Béguin, *Electrochem. Commun.*, 2010, **12**, 414–417.
- 194 C.-T. Hsieh and H. Teng, *Carbon*, 2002, **40**, 667–674.
- 195 Y.-J. Kim, B.-J. Lee, H. Suezaki, T. Chino, Y. Abe, T. Yanagiura, K. C. Park and M. Endo, *Carbon*, 2006, **44**, 1592–1595.
- 196 D. Qu and H. Shi, *J. Power Sources*, 1998, **74**, 99–107.
- 197 M. Olivares-Marín, J. A. Fernández, M. J. Lázaro, C. Fernández-González, A. Macías-García, V. Gómez-Serrano, F. Stoeckli and T. A. Centeno, *Mater. Chem. Phys.*, 2009, **114**, 323–327.
- 198 Z. Li, L. Zhang, B. S. Amirkhiz, X. Tan, Z. Xu, H. Wang, B. C. Olsen, C. M. B. Holt and D. Mitlin, *Adv. Energy Mater.*, 2012, **2**, 431–437.
- 199 D. Hulicova-Jurcakova, M. Seredych, G. Q. Lu and T. J. Bandoz, *Adv. Funct. Mater.*, 2009, **19**, 438–447.
- 200 Y.-H. Lee, K.-H. Chang and C.-C. Hu, *J. Power Sources*, 2013, **227**, 300–308.
- 201 J. Jiang, J. Zhu, W. Ai, Z. Fan, X. Shen, C. Zou, J. Liu, H. Zhang and T. Yu, *Energy Environ. Sci.*, 2014, **7**, 2670–2679.
- 202 D. Hulicova-Jurcakova, A. M. Puziy, O. I. Poddubnaya, F. Suárez-García, J. M. D. Tascón and G. Q. Lu, *J. Am. Chem. Soc.*, 2009, **131**, 5026–5027.
- 203 L. Cheng, P. Guo, R. Wang, L. Ming, F. Leng, H. Li and X. S. Zhao, *Colloids Surf., A*, 2014, **446**, 127–133.
- 204 C. Huang, A. M. Puziy, T. Sun, O. I. Poddubnaya, F. Suárez-García, J. M. D. Tascón and D. Hulicova-Jurcakova, *Electrochim. Acta*, 2014, **137**, 219–227.
- 205 L.-F. Chen, Z.-H. Huang, H.-W. Liang, Q.-F. Guan and S.-H. Yu, *Adv. Mater.*, 2013, **25**, 4746–4752.
- 206 J. C. Bachman, S. Muy, A. Grimaud, H.-H. Chang, N. Pour, S. F. Lux, O. Paschos, F. Maglia, S. Lupart, P. Lamp, L. Giordano and Y. Shao-Horn, *Chem. Rev.*, 2016, **116**, 140–162.
- 207 X.-B. Cheng, R. Zhang, C.-Z. Zhao and Q. Zhang, *Chem. Rev.*, 2017, **117**, 10403–10473.
- 208 M. S. Whittingham, *Chem. Rev.*, 2004, **104**, 4271–4302.
- 209 X. Rui, H. Tan and Q. Yan, *Nanoscale*, 2014, **6**, 9889–9924.
- 210 H. Wang, W. Yu, J. Shi, N. Mao, S. Chen and W. Liu, *Electrochim. Acta*, 2016, **188**, 103–110.
- 211 W. Tang, Y. Zhang, Y. Zhong, T. Shen, X. Wang, X. Xia and J. Tu, *Mater. Res. Bull.*, 2017, **88**, 234–241.
- 212 X. Zhou, F. Chen, T. Bai, B. Long, Q. Liao, Y. Ren and J. Yang, *Green Chem.*, 2016, **18**, 2078–2088.
- 213 J. Hou, C. Cao, F. Idrees and X. Ma, *ACS Nano*, 2015, **9**, 2556–2564.
- 214 L. Yan, J. Yu, J. Houston, N. Flores and H. Luo, *Green Energy Environ.*, 2017, **2**, 84–99.
- 215 C. Ma, X. Shao and D. Cao, *J. Mater. Chem.*, 2012, **22**, 8911–8915.
- 216 Z. Li, Z. Xu, X. Tan, H. Wang, C. M. Holt, T. Stephenson, B. C. Olsen and D. Mitlin, *Energy Environ. Sci.*, 2013, **6**, 871–878.
- 217 F. Cheng, W.-C. Li and A.-H. Lu, *ACS Appl. Mater. Interfaces*, 2016, **8**, 27843–27849.
- 218 L. Wang, Y. Zheng, X. Wang, S. Chen, F. Xu, L. Zuo, J. Wu, L. Sun, Z. Li and H. Hou, *ACS Appl. Mater. Interfaces*, 2014, **6**, 7117–7125.
- 219 X. Zhu, G. Ning, X. Ma, Z. Fan, C. Xu, J. Gao, C. Xu and F. Wei, *J. Mater. Chem. A*, 2013, **1**, 14023–14030.
- 220 B. Jang, M. Park, O. B. Chae, S. Park, Y. Kim, S. M. Oh, Y. Piao and T. Hyeon, *J. Am. Chem. Soc.*, 2012, **134**, 15010–15015.
- 221 A. L. M. Reddy, M. M. Shaijumon, S. R. Gowda and P. M. Ajayan, *Nano Lett.*, 2009, **9**, 1002–1006.
- 222 Y. Chen, Z. Lu, L. Zhou, Y.-W. Mai and H. Huang, *Nanoscale*, 2012, **4**, 6800–6805.
- 223 S. Xin, Y.-G. Guo and L.-J. Wan, *Acc. Chem. Res.*, 2012, **45**, 1759–1769.
- 224 S. Gu, C. Sun, D. Xu, Y. Lu, J. Jin and Z. Wen, *Electrochem. Energy Rev.*, 2018, 1–26.
- 225 J. Balach, J. Linnemann, T. Jaumann and L. Giebeler, *J. Mater. Chem. A*, 2018, **6**, 23127–23168.
- 226 H. Yuan, J. Q. Huang, H. J. Peng, M. M. Titirici, R. Xiang, R. Chen, Q. Liu and Q. Zhang, *Adv. Energy Mater.*, 2018, 1802107.
- 227 A. Manthiram, Y. Fu, S.-H. Chung, C. Zu and Y.-S. Su, *Chem. Rev.*, 2014, **114**, 11751–11787.
- 228 A. Manthiram, Y. Fu and Y.-S. Su, *Acc. Chem. Res.*, 2012, **46**, 1125–1134.
- 229 L. Zhang, Y. Wang, Z. Niu and J. Chen, *Carbon*, 2019, **141**, 400–416.
- 230 M. Wang, X. Xia, Y. Zhong, J. Wu, R. Xu, Z. Yao, D. Wang, W. Tang, X. Wang and J. Tu, *Chem. – Eur. J.*, 2019, **25**, 3710–3725.
- 231 T. Tang and Y. Hou, *Electrochem. Energy Rev.*, 2018, 1–30.
- 232 J. Zhu, R. Pitcheri, T. Kang, C. Jiao, Y. Guo, J. Li and Y. Qiu, *J. Electroanal. Chem.*, 2019, **833**, 151–159.
- 233 S. Luo, W. Sun, J. Ke, Y. Wang, S. K. Liu, X. Hong, Y. Li, Y. Chen, W. Xie and C. Zheng, *Nanoscale*, 2018, **10**, 22601–22611.
- 234 X. Qin, J. Wu, Z.-L. Xu, W. G. Chong, J.-Q. Huang, G. Liang, B. Li, F. Kang and J.-K. Kim, *Carbon*, 2019, **141**, 16–24.
- 235 X. Liang, C. Y. Kwok, F. Lodi-Marzano, Q. Pang, M. Cuisinier, H. Huang, C. J. Hart, D. Houtarde, K. Kaup and H. Sommer, *Adv. Energy Mater.*, 2016, **6**, 1501636.
- 236 Q. Pang, X. Liang, C. Y. Kwok and L. F. Nazar, *Nat. Energy*, 2016, **1**, 16132.
- 237 X. Liu, J. Q. Huang, Q. Zhang and L. Mai, *Adv. Mater.*, 2017, **29**, 1601759.
- 238 H. Pan, Y.-S. Hu and L. Chen, *Energy Environ. Sci.*, 2013, **6**, 2338–2360.
- 239 X. Zhou and Y.-G. Guo, *ChemElectroChem*, 2014, **1**, 83–86.
- 240 M.-S. Balogun, Y. Luo, W. Qiu, P. Liu and Y. Tong, *Carbon*, 2016, **98**, 162–178.
- 241 Y. Yao and F. Wu, *Nano Energy*, 2015, **17**, 91–103.
- 242 E. M. Lotfabad, J. Ding, K. Cui, A. Kohandehghan, W. P. Kalisvaart, M. Hazelton and D. Mitlin, *ACS Nano*, 2014, **8**, 7115–7129.
- 243 J. Tang, V. Etacheri and V. G. Pol, *Sci. Rep.*, 2016, **6**, 20290.
- 244 K.-L. Hong, L. Qie, R. Zeng, Z.-Q. Yi, W. Zhang, D. Wang, W. Yin, C. Wu, Q.-J. Fan, W.-X. Zhang and Y.-H. Huang, *J. Mater. Chem. A*, 2014, **2**, 12733–12738.

- 245 H. Ru, N. Bai, K. Xiang, W. Zhou, H. Chen and X. S. Zhao, *Electrochim. Acta*, 2016, **194**, 10–16.
- 246 L. Wei, M. Sevilla, A. B. Fuertes, R. Mokaya and G. Yushin, *Adv. Energy Mater.*, 2011, **1**, 356–361.
- 247 J. Ding, H. Wang, Z. Li, A. Kohandehghan, K. Cui, Z. Xu, B. Zahiri, X. Tan, E. M. Lotfabad, B. C. Olsen and D. Mitlin, *ACS Nano*, 2013, **7**, 11004–11015.
- 248 W. Li, J. Huang, L. Feng, L. Cao, Y. Ren, R. Li, Z. Xu, J. Li and C. Yao, *J. Alloys Compd.*, 2017, **716**, 210–219.
- 249 S. Cao and J. Yu, *J. Photochem. Photobiol., C*, 2016, **27**, 72–99.
- 250 L. Wang, Z. Yao, F. Jia, B. Chen and Z. Jiang, *Dalton Trans.*, 2013, **42**, 9976–9981.
- 251 Q. Xiang, J. Yu and M. Jaroniec, *Chem. Soc. Rev.*, 2012, **41**, 782.
- 252 K. S. Fernando, S. Sahu, Y. Liu, W. K. Lewis, E. A. Gulians, A. Jafariyan, P. Wang, C. E. Bunker and Y.-P. Sun, *ACS Appl. Mater. Interfaces*, 2015, **7**, 8363–8376.
- 253 Y. Fang, C. Bi, D. Wang and J. Huang, *ACS Energy Lett.*, 2017, **2**, 782–794.
- 254 A. Hagfeldt, G. Boschloo, L. Sun, L. Kloo and H. Pettersson, *Chem. Rev.*, 2010, **110**, 6595–6663.
- 255 Y. H. Jang, Y. J. Jang, S. Kim, L. N. Quan, K. Chung and D. H. Kim, *Chem. Rev.*, 2016, **116**, 14982–15034.
- 256 K. P. Loh, S. W. Tong and J. Wu, *J. Am. Chem. Soc.*, 2016, **138**, 1095–1102.
- 257 J. Briscoe, A. Marinovic, M. Sevilla, S. Dunn and M. Titirici, *Angew. Chem., Int. Ed.*, 2015, **54**, 4463–4468.
- 258 J. Chen, X. Gui, Z. Wang, Z. Li, R. Xiang, K. Wang, D. Wu, X. Xia, Y. Zhou, Q. Wang, Z. Tang and L. Chen, *ACS Appl. Mater. Interfaces*, 2012, **4**, 81–86.
- 259 J. Choi, Y. Jung, S. J. Yang, J. Y. Oh, J. Oh, K. Jo, J. G. Son, S. E. Moon, C. R. Park and H. Kim, *ACS Nano*, 2017, **11**, 7608–7614.
- 260 S. L. Kim, K. Choi, A. Tazebay and C. Yu, *ACS Nano*, 2014, **8**, 2377–2386.
- 261 C. A. Hewitt, A. B. Kaiser, S. Roth, M. Craps, R. Czerw and D. L. Carroll, *Nano Lett.*, 2012, **12**, 1307–1310.